

GADGET: A code for collisionless and gasdynamical cosmological simulations¹

Volker Springel^{1,2}, Naoki Yoshida¹ and Simon D. M. White¹

¹Max-Planck-Institut für Astrophysik, Karl-Schwarzschild-Straße 1, 85740 Garching bei München, Germany

²Harvard-Smithsonian Center for Astrophysics, 60 Garden Street, Cambridge, MA 02138, USA

Abstract

We describe the newly written code GADGET which is suitable both for cosmological simulations of structure formation and for the simulation of interacting galaxies. GADGET evolves self-gravitating collisionless fluids with the traditional N-body approach, and a collisional gas by smoothed particle hydrodynamics. Along with the serial version of the code, we discuss a parallel version that has been designed to run on massively parallel supercomputers with distributed memory. While both versions use a tree algorithm to compute gravitational forces, the serial version of GADGET can optionally employ the special-purpose hardware GRAPE instead of the tree. Periodic boundary conditions are supported by means of an Ewald summation technique. The code uses individual and adaptive timesteps for all particles, and it combines this with a scheme for dynamic tree updates. Due to its Lagrangian nature, GADGET thus allows a very large dynamic range to be bridged, both in space and time. So far, GADGET has been successfully used to run simulations with up to 7.5×10^7 particles, including cosmological studies of large-scale structure formation, high-resolution simulations of the formation of clusters of galaxies, as well as workstation-sized problems of interacting galaxies. In this study, we detail the numerical algorithms employed, and show various tests of the code. We publically release both the serial and the massively parallel version of the code.

Key words: methods: numerical – galaxies: interactions – cosmology: dark matter.

1. Introduction

Numerical simulations of three-dimensional self-gravitating fluids have become an indispensable tool in cosmology. They are now routinely used to study the non-linear gravitational clustering of dark matter, the formation of clusters of galaxies, the interactions of isolated galaxies, and the evolution of the intergalactic gas. Without numerical techniques the immense progress made in these fields recently would have been impossible, since analytic calculations are often restricted to idealized problems of high symmetry, or to approximate treatments of inherently nonlinear problems.

The advances in numerical simulations have become possible both by the rapid growth of computer performance and also by the implementation of ever more sophisticated numerical algorithms. Note that the development of powerful simulation codes still remains a primary task if one wants to take full advantage of new computer technologies.

While the direct summation method for the gravitational N-body problem remains useful in small stellar dynamical systems, it is hopelessly inefficient for large N due to the $\mathcal{O}(N^2)$ scaling of its computational cost. A large number of

groups have therefore developed N-body codes that compute the large-scale gravitational field by means of Fourier techniques. These are the PM, P³M, and AP³M codes (Efstathiou et al., 1985; Couchman, 1991; Kravtsov et al., 1997; MacFarland et al., 1998). The modern versions of these codes supplement the force computation on scales below the mesh size with a direct summation, and they place mesh refinements on highly clustered regions.

An alternative to these schemes are the so-called tree algorithms, pioneered by Barnes & Hut (1986) and Jernigan & Porter (1989). Tree algorithms arrange particles in a hierarchy of groups, and compute the gravitational field at a given point by summing over multipole expansions of these groups. In this way the computational cost of a complete force evaluation can be reduced to a $\mathcal{O}(N \log N)$ scaling.

While mesh-based codes are generally much faster for close-to-homogeneous particle distributions, the tree codes can adapt flexibly to any clustering state without significant losses in speed. This Lagrangian nature is a great advantage, if a large dynamic range in density needs to be covered. Here tree codes can outperform mesh based algorithms. In addition, tree codes are free from any geometrical restrictions,

and they have been successfully combined with integration schemes that advance particles on individual timesteps.

Recently, first attempts have been made to combine PM and tree solvers into hybrid Tree-PM codes (Bagla, 1999; Bode et al., 1999). In this approach, the speed and accuracy of the PM method for the large-range part of the gravitational force is combined with a computation of the short-range force by a gravitational tree. This may be seen as a replacement of the direct summation PP part in P^3M codes with a tree algorithm. The Tree-PM technique is clearly a very promising new method, especially if large cosmological volumes with strong clustering on small scales are studied.

Yet another solution to the N-body problem is provided by special-purpose hardware like the GRAPE board (Makino & Funato, 1993; Ebisuzaki et al., 1993; Steinmetz, 1996; Makino et al., 1997; Athanassoula et al., 1998). It consists of custom chips that compute gravitational forces by the direct summation technique. By means of their enormous computational speed they can considerably extend the range where direct summation remains competitive with software solutions.

In recent years, collisionless dynamics has also been coupled to gas dynamics, establishing a more direct link between dark matter and observable quantities. Traditionally, hydrodynamical simulations have usually employed some kind of mesh to represent fluid dynamical quantities. While a particular strength of these codes is their ability to accurately resolve shocks, the mesh also imposes restrictions on the geometry of the problem, and onto the dynamic range of spatial scales that can be simulated. However, new adaptive mesh refinement codes of Norman & Bryan (1998) and Klein et al. (1998) may provide a solution to this problem.

In cosmological applications, it is often sufficient to describe the gas by smoothed particle hydrodynamics (SPH), as invented by Lucy (1977) and Gingold & Monaghan (1977). The particle-based SPH is extremely flexible in its ability to adapt to any given geometry. Moreover, its Lagrangian nature allows a locally changing resolution that ‘automatically’ follows the local mass density. This convenient feature helps to save computing time by concentrating the computational effort on those regions that have the largest gas concentrations. Furthermore, SPH ties naturally into the N-body approach for self-gravity, and can be easily implemented in three dimensions.

These advantages have led a number of authors to develop SPH codes for applications in cosmology. Among them are TREESPH (Hernquist & Katz, 1989; Katz et al., 1996), GRAPESPH (Steinmetz, 1996), HYDRA (Couchman et al., 1995; Pearce & Couchman, 1997), and codes by Evrard (1988); Navarro & White (1993); Hultman & Källander (1997); Davé et al. (1997); Carraro et al. (1998). See also Kang et al. (1994) and Frenk et al. (1999) for a comparison of cosmological hydrodynamic codes.

In this work we describe our simulation code GADGET (GAlaxies with Dark matter and Gas intEraCT), which can

be used both to simulate isolated self-gravitating systems including gas, or for cosmological N-body/SPH simulations. We have developed two versions of this code, a serial workstation version, and a version for massively parallel supercomputers with distributed memory. The workstation code uses either a tree algorithm for the self-gravity, or the special purpose hardware GRAPE, if available. The parallel version works with a tree only. Note that the parallelization required substantial algorithmic changes compared to the serial code.

A particular emphasis of our work has been the development of an efficient time integration scheme that allows individual and adaptive particle timesteps, and on the elimination of sources of overhead both in the serial and parallel code. We have investigated different time step criteria, and have come up with a number of algorithmic improvements that speed up the code, while maintaining its accuracy. As a result, GADGET is a very flexible code without obvious intrinsic restrictions for the dynamic range of the problems that can be addressed with it. We release the parallel version of the code on the internet¹, hoping that it will be useful for people working on cosmological simulations, and that it will stimulate further code development efforts in the community.

In this work we describe in detail the implemented equations and algorithms of our code(s), and we show results for some test problems and science applications. In Section 2, we give a brief summary of the implemented physics. In Section 3, we discuss the computation of the gravitational force both with a tree algorithm, and with GRAPE. We then describe our specific implementation of SPH in Section 4, and we discuss our time integration scheme in Section 5. The parallelization of the code is described in Section 6, and tests of the code are presented in Section 7. Finally, we summarize in Section 8.

2. Implemented physics

2.1. Collisionless dynamics

Dark matter and stars are modeled as self-gravitating collisionless fluids, i.e. they fulfill the collisionless Boltzmann equation (CBE)

$$\frac{df}{dt} \equiv \frac{\partial f}{\partial t} + \mathbf{v} \cdot \frac{\partial f}{\partial \mathbf{x}} - \frac{\partial \Phi}{\partial \mathbf{r}} \frac{\partial f}{\partial \mathbf{v}} = 0, \quad (1)$$

where the self-consistent potential Φ is the solution of Poisson’s equation

$$\nabla^2 \Phi(\mathbf{r}, t) = 4\pi G \int f(\mathbf{r}, \mathbf{v}, t) d\mathbf{v}, \quad (2)$$

and $f(\mathbf{r}, \mathbf{v}, t)$ is the mass density in single-particle phase-space. It is exceedingly difficult to solve this coupled system of equations directly with finite difference methods. Instead, we will follow the common N-body approach, where

¹GADGET’s web-site is:

<http://www.mpa-garching.mpg.de/~volker/gadget>

the phase fluid is represented by N particles which are integrated along the characteristic curves of the CBE. In essence, this is a Monte Carlo approach whose accuracy depends crucially on a sufficiently high number of particles.

The N-body problem is thus the task of following Newton's equation of motion for a large number of particles under their own self-gravity. Note that we will introduce a softening into the gravitational potential at small separations. This effectively introduces a lower spatial resolution cut-off, which is necessary to suppress large-angle scattering in two-body collisions. It also allows larger integration timesteps, and prolongs the relaxation time of the system due to two-body encounters.

2.2. Gasdynamics

A simple description of the intergalactic medium (IGM), or the interstellar medium (ISM), may be obtained by modeling it as an ideal, inviscid gas. The gas is then governed by the continuity equation

$$\frac{d\rho}{dt} + \rho \nabla \cdot \mathbf{v} = 0, \quad (3)$$

and the Euler equation

$$\frac{dv}{dt} = -\frac{\nabla P}{\rho} - \nabla \Phi. \quad (4)$$

Further, the thermal energy u per unit mass evolves according to the first law of thermodynamics, viz.

$$\frac{du}{dt} = -\frac{P}{\rho} \nabla \cdot \mathbf{v} - \frac{\Lambda(u, \rho)}{\rho}. \quad (5)$$

Here we used Lagrangian time derivatives, i.e.

$$\frac{d}{dt} = \frac{\partial}{\partial t} + \mathbf{v} \cdot \nabla, \quad (6)$$

and we allowed for a piece of ‘extra’ physics in form of the *cooling function* $\Lambda(u, \rho)$, describing external sinks or sources of heat for the gas.

For a simple ideal gas, the equation of state is

$$P = (\gamma - 1)\rho u, \quad (7)$$

where γ is the adiabatic exponent. We usually take $\gamma = 5/3$, appropriate for a mono-atomic ideal gas. The adiabatic sound speed c of this gas is $c^2 = \gamma P/\rho$.

3. Gravity

3.1. Tree algorithm

An alternative to Fourier techniques, or to direct summation, are the so-called tree methods. In these schemes the particles are arranged in a hierarchy of groups. When the force on

a particular particle is computed the force exerted by distant groups is approximated by their lowest multipole moments. Usually this approximation is terminated at quadrupole order. Tree codes are a class of algorithms that in this way reduce the computational cost for a complete force evaluation to $\mathcal{O}(N \log N)$ (Jernigan & Porter, 1989; Barnes & Hut, 1986).

We employ the Barnes & Hut (1986, BH) tree in this work. In this scheme, the computational domain is hierarchically partitioned into a sequence of cubes, where each cube contains eight siblings, each with half the side-length of the parent cube. These cubes form the nodes of an oct-tree structure. The tree is constructed such that each node (cube) contains either exactly one particle, or is progenitor to further nodes, in which case the node carries the monopole and quadrupole moments of all the particles that lie inside its cube. A schematic illustration of the BH tree is shown in Figure 1.

A force computation then proceeds by walking the tree, and summing up appropriate force contributions from tree nodes. In the standard BH tree walk, the multipole expansion of a node of size l is used only if

$$r > \frac{l}{\theta}, \quad (8)$$

where r is the distance of the point of reference to the center-of-mass of the cell and θ is a prescribed accuracy parameter. If a node fulfills the criterion (8), the tree walk along this branch can be terminated, otherwise it is ‘opened’, and the walk is continued with all its siblings. Following Dubinski et al. (1996) we have also tried the simple modification

$$r > \frac{l}{\theta} + \delta, \quad (9)$$

of the opening criterion, where the quantity δ gives the distance of the geometric center of the cell to its center-of-mass. This provides protection against pathological cases where the center-of-mass lies close to an edge of a cell. However, except for the first force computation in a simulation, we will usually employ yet another opening criterion which tries to limit the absolute error in every particle-node interaction. We will discuss this in more detail in Section 3.3.

A technical difficulty arises when the gravity is softened. In regions of high particle density (e.g. centers of dark haloes, or cold dense gas knots in dissipative simulations), it can frequently happen that nodes fulfill equation (8), and simultaneously one has $r < h$, where h is the gravitational softening length. In this situation, one formally needs the multipole moments of the *softened* gravitational field. Some previous tree codes have ignored this complication altogether, or they have opened nodes always for $r < h$. The first solution can lead to forces significantly in error, while the latter can suffer from severe (and unnecessary) performance degradation for strongly clustered regions (Hernquist & Katz, 1989).

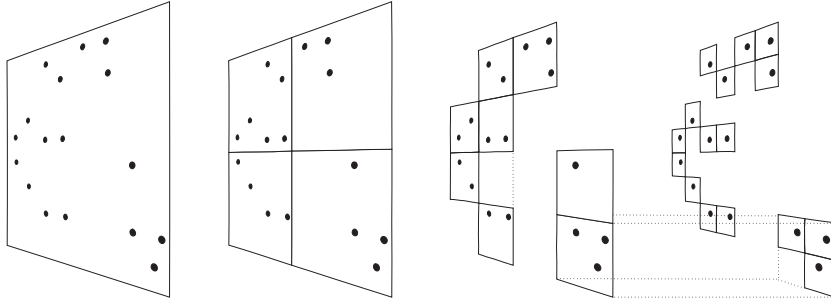


Figure 1: Schematic illustration of the Barnes & Hut oct-tree in two dimensions. The particles are first enclosed in a square (root node). This square is then iteratively subdivided in four squares of half the size, until exactly one particle is left in each final square (leaves of the tree). In the resulting tree structure, each square can be progenitor of up to four siblings. Note that empty squares need not to be stored.

However, it is possible to do the proper multipole expansion for the softened potential, and we now discuss it for definiteness. We want to approximate the potential at \mathbf{r} due to a (distant) bunch of particles with masses m_i and coordinates \mathbf{x}_i . Note that we use a spline-softened force law, hence the exact potential of the particle group is

$$\Phi(\mathbf{r}) = -G \sum_k m_k g(|\mathbf{x}_k - \mathbf{r}|), \quad (10)$$

where the function $g(r)$ describes the softened force law. For Newtonian gravity we have $g(r) = 1/r$, while the spline softened gravity with softening length h gives rise to

$$g(r) = -\frac{1}{h} W_2\left(\frac{r}{h}\right). \quad (11)$$

The function $W_2(u)$ is given in the Appendix. It arises by replacing the force due to a point mass m with the force exerted by the mass distribution $\rho(\mathbf{r}) = mW(\mathbf{r}; h)$, where we take $W(r; h)$ to be the normalized spline kernel used in the SPH formalism.

The spline softening has the advantage that the force becomes exactly Newtonian for $r > h$, while other possible force laws, like the Plummer softening to be discussed below, often converge only relatively slowly to Newton's law.

We now introduce the center-of-mass \mathbf{s} , and the total mass M of the particles. Further we define

$$\mathbf{y} \equiv \mathbf{r} - \mathbf{s}. \quad (12)$$

The potential may then be expanded in a multipole series assuming $|\mathbf{y}| \gg |\mathbf{x}_k - \mathbf{s}|$. Up to quadrupole order, this results in

$$\begin{aligned} \Phi(\mathbf{r}) = & -G \left\{ Mg(y) \right. \\ & \left. + \frac{1}{2} \mathbf{y}^T \left[\frac{g''(y)}{y^2} \mathbf{Q} + \frac{g'(y)}{y^3} (\mathbf{P} - \mathbf{Q}) \right] \mathbf{y} \right\}. \end{aligned} \quad (13)$$

Here we have introduced the tensors

$$\mathbf{Q} = \sum_k m_k (\mathbf{x}_k - \mathbf{s})(\mathbf{x}_k - \mathbf{s})^T = \sum_k m_k \mathbf{x}_k \mathbf{x}_k^T - M \mathbf{s} \mathbf{s}^T, \quad (14)$$

and

$$\mathbf{P} = \mathbf{I} \sum_k m_k (\mathbf{x}_k - \mathbf{s})^2 = \mathbf{I} \left[\sum_k m_k \mathbf{x}_k^2 - M \mathbf{s}^2 \right], \quad (15)$$

where \mathbf{I} is the unit matrix. Note that for Newtonian gravity, equation (13) reduces to the perhaps more familiar form

$$\Phi(\mathbf{r}) = -G \left[\frac{M}{y} + \frac{1}{2} \mathbf{y}^T \frac{3\mathbf{Q} - \mathbf{P}}{y^5} \mathbf{y} \right]. \quad (16)$$

Finally, the quadrupole approximation of the softened gravitational field is given by

$$\begin{aligned} \mathbf{f}(\mathbf{r}) = -\nabla \Phi = & G \left\{ Mg_1(y) \mathbf{y} + g_2(y) \mathbf{Q} \mathbf{y} \right. \\ & \left. + \frac{1}{2} g_3(y) (\mathbf{y}^T \mathbf{Q} \mathbf{y}) \mathbf{y} + \frac{1}{2} g_4(y) \mathbf{P} \mathbf{y} \right\}. \end{aligned} \quad (17)$$

Here we introduced the functions $g_1(y)$, $g_2(y)$, $g_3(y)$, and $g_4(y)$ as convenient abbreviations. Their definition is given in the appendix. In the Newtonian case, this simplifies to

$$\mathbf{f}(\mathbf{r}) = G \left\{ -\frac{M}{y^3} \mathbf{y} + \frac{3\mathbf{Q}}{y^5} \mathbf{y} - \frac{15}{2} \frac{\mathbf{y}^T \mathbf{Q} \mathbf{y}}{y^7} \mathbf{y} + \frac{3}{2} \frac{\mathbf{P}}{y^5} \mathbf{y} \right\}. \quad (18)$$

Note that although equation (17) looks rather cumbersome, its actual numerical computation is only marginally more expansive than that of the Newtonian form (18) because all factors involving $g(y)$ and derivatives thereof can be tabulated for later use in repeated force calculations.

3.2. Tree construction and tree walks

The tree construction can be done by inserting the particles one after the other in the tree. It is possible to compute the multipole moments simultaneously by summing the

$\sum_k m_k x_i^{(k)} x_j^{(k)}$ terms for each node, and then looping at the end over all nodes again and subtracting the corresponding center-of-mass moments. However, if single-precision floating point numbers are used for the storage of node properties, this procedure can result in intolerable accuracy losses when the number of particles in a node is large and the nodes' distance to the coordinate origin is large compared to its sidelength. In this case, the multipole moments arise as a small difference between two large numbers, a situation that can easily outrun the dynamic range of single precision arithmetic. A better solution is obtained by referring the particle coordinates to a fixed point inside the node (e.g. the geometrical center), a procedure we employ in our tree construction. In addition, we use double precision arithmetic for the computation of the multipole moments, even though they are stored in single precision. For this purpose the tree construction is done in two steps. In the first pass, we just construct the hierarchical grouping of the tree, and in a second pass we compute the multipole moments of each internal node, using a link-list structure to access all the particles represented by each of them. This link-list structure will also be used for dynamical updates of parts of the tree, and for the neighbour search in SPH.

The tree-construction is very fast, and the time spent for it is negligible compared to a complete force walk for all particles. However, in our time integration scheme we use individual timesteps for all particles, and at each given timestep, only a small fraction of all particles require a force walk. If this fraction drops below ~ 1 per cent, a full reconstruction of the tree can take as long as the force walk itself. However, most of this tree construction time can be eliminated by dynamic tree updates, which we discuss in more detail in Section 5. The most time consuming routine in the code will then always be the tree walk, and optimizing it can considerably speed up tree codes. Interestingly, in the grouping technique of Barnes, the speed of the gravitational force computation can be increased by performing a common tree-walk for a localized group of particles. Even though the average length of the interaction list for each particles becomes larger in this way, this can be offset by saving some of the tree-walk overhead. Unfortunately, this advantage is not easily kept if adaptive timesteps are used where only a small fraction of the particles are active, so we do not use grouping.

GADGET allows different gravitational softenings for particles of different 'type'. In order to guarantee momentum conservation, this requires a symmetrization of the force when particles with different softening lengths interact. We here chose to symmetrize the softenings by

$$h = \max(h_i, h_j). \quad (19)$$

However, the usage of different softening lengths leads to complications for softened tree nodes. Strictly speaking, the multipole expansion is only possible if all the particles in the

node have the same softening. GADGET solves this problem by constructing separate trees for each species of particles with different softening. As long as these species are more or less spatially separated (e.g. dark halo, stellar disk, and stellar bulge in simulations of interacting galaxies), no severe performance penalty results. However, this is different if the fluids are spatially well 'mixed'. Here a single tree would result in higher performance of the gravity computation, so it is advisable to choose a single softening in this case. Note that for SPH particles we nevertheless always create a separate tree to allow its use for a fast neighbour search, as will be discussed below.

3.3. A new opening criterion

The accuracy of the forces resulting from the tree walk depends sensitively on the criterion used to decide whether the multipole approximation for a given node is acceptable, or whether the node has to be 'opened' for further refinement. The standard BH opening criterion tries to limit the relative error of every particle-node interaction by comparing a rough estimate of the size of the quadrupole term, $\sim Ml^2/r^4$, with the size of the monopole term, $\sim M/r^2$. The result is the purely geometrical criterion of equation (8).

As Salmon & Warren (1994) have pointed out, the worst-case behaviour of the BH opening criterion is somewhat worrying. Although very rare in real astrophysical simulations, the BH criterion can occasionally lead to very large force errors, when standard values for the opening angle are used.

Another problem with the BH criterion occurs when one tries to use it at high redshift in cosmological simulations. Here, the density field is very close to homogeneous and the peculiar acceleration is small. For a tree algorithm this is a tough problem, because the tree code always has to sum up partial forces from *all* the mass in a simulation. The small net force at high z then arises in a delicate cancellation process between relatively large partial forces. If a partial force is indeed much larger than the net force, even a small *relative* error in it is enough to result in a large relative error of the net force. For an unclustered particle distribution, the BH criterion therefore requires a much smaller value of the opening angle than for a clustered one.

Similarly, in a cosmological simulation the absolute sizes of forces between a given particle and tree-nodes of a certain opening angle can vary by many orders of magnitude. In this situation, the purely geometrical BH criterion ends up investing a lot of computational effort for the evaluation of all partial forces to the same relative accuracy, irrespective of the actual size of each partial force, and the size of the *absolute* error thus induced. It would be better to invest more computational effort in regions that provide most of the force on the particle and less in regions whose mass content is unimportant for the total force.

As suggested by Salmon & Warren (1994), one may there-

fore try to devise a cell-opening criterion that limits the absolute error in every cell-particle interaction. In principle, one may use analytic error bounds (Salmon & Warren, 1994) to obtain a suitable cell-opening criterion, but the evaluation of the relevant expressions can consume significant amounts of CPU time.

Our approach to a new opening criterion is less stringent. Assume the absolute size of the true total force is already known before the tree walk. In our code, we will use the acceleration of the previous timestep as a handy approximate value for that. We will now require that the estimated error of an acceptable multipole approximation is some small fraction of this total force. Note that we truncate the multipole expansion at quadrupole order. If the hexadecapole order is the leading term in the neglected part of the series, the absolute truncation error will be roughly of the size of this term, which is of order $\simeq M/r^2(l/r)^4$. We can then require that this error should not exceed some fraction α of the total force on the particle. The latter may be estimated from the previous timestep. A tree-node has then to be opened if

$$M l^4 > \alpha |\mathbf{a}_{\text{old}}| r^6. \quad (20)$$

We have found this criterion to be more efficient than the ordinary BH criterion, i.e. at a given computational expense it produces forces that are more accurate. Also, this criterion does not suffer from the high- z problem discussed above. The same value of α produces a comparable force accuracy, independent of the clustering state of the material. In Section 7.2, we will show some quantitative measurements of the relative performance of the two criteria, and compare it to the optimum cell-opening strategy.

3.4. Special purpose hardware

An alternative to software solutions to the N^2 -bottleneck of self-gravity is provided by the GRAPE (GRAvity PipE) special-purpose hardware. It is designed to solve the gravitational N-body problem in a direct summation, brute-force approach by means of its superior computational speed. The latter is achieved with custom chips that compute the gravitational force with a hardwired Plummer force law. The Plummer-potential of GRAPE takes the form

$$\Phi(\mathbf{r}) = -G \sum_j \frac{m_j}{(|\mathbf{r} - \mathbf{r}_j|^2 + \epsilon^2)^{\frac{1}{2}}}. \quad (21)$$

As an example, the GRAPE-3A boards installed at the MPA in 1998 have 40 N-body integrator chips in total with an approximate peak performance of 25 GFlops. Recently, newer generations of GRAPE boards have achieved even higher computational speeds. In fact, with the GRAPE-4 the 1 TFlop barrier was already broken (Makino et al., 1997), and even faster special-purpose machines are in preparation (Spurzem, 1997).

The GRAPE-3A boards are connected to an ordinary workstation via a VME or PCI interface. The boards consist of memory chips that can hold up to 131072 particle coordinates, and of integrator chips that can compute the forces exerted by these particles for 40 positions in parallel. Note that higher particle numbers can also be processed by splitting them up in sufficiently small groups. In addition to the gravitational force, the GRAPE board returns the potential, and a list of neighbours for the 40 positions within search radii h_i specified by the user. This latter feature makes GRAPE attractive also for SPH calculations.

The parts of our code that use GRAPE have benefited from the code GRAPESPH by Steinmetz (1996), and are similar to it. In short, the usage of GRAPE proceeds as follows. For the force computation, the particle coordinates are first loaded onto the GRAPE board, then GADGET calls GRAPE repeatedly to compute the force for up to 40 positions in parallel. The communication with GRAPE is done by means of a convenient software interface in C. GRAPE can also provide lists of nearest neighbours. For SPH-particles, GADGET computes the gravitational force and the interaction list in just one call of GRAPE. The host computer then still does the rest of the work, i.e. it advances the particles, and computes the hydrodynamical forces.

In practice, there are some technical complications when one works with GRAPE. In order to achieve high computational speed, the GRAPE hardware works internally with special fixed-point formats for positions, accelerations and masses. This results in a reduced dynamic range compared to standard IEEE floating point arithmetic. In particular, one needs to specify a minimum length scale d_{\min} and a minimum mass scale m_{\min} when working with GRAPE. The spatial dynamic range is then given by $d_{\min}[-2^{18}; 2^{18}]$ and the mass range is $m_{\min}[1; 64\epsilon/d_{\min}]$ (Steinmetz, 1996). In GADGET we take special care that these constraints are always observed, otherwise the simulation could be compromised by numerical errors.

While the communication time with GRAPE scales proportional to the particle number N , the actual force computation of GRAPE is still an $\mathcal{O}(N^2)$ -algorithm, because the GRAPE board implements a brute-force approach to the gravitational N-body problem. This implies that for very large particle number a tree code running on the workstation alone will eventually catch up and outperform the combination of workstation and GRAPE. For our current set-up at MPA this break-even point is about 300000 particles.

However, it seems also possible to combine GRAPE with a tree algorithm (Fukushige et al., 1991; Athanassoula et al., 1998), for example by exporting tree nodes instead of particles in an appropriate way. Such a combination of tree+GRAPE could scale as $\mathcal{O}(N \log N)$ and should be able to outperform pure software solutions even for large N .

4. Smoothed particle hydrodynamics

SPH is a powerful Lagrangian technique to solve hydrodynamical problems with an ease that is unmatched by grid based fluid solvers (see Monaghan, 1992, for an excellent review). In particular, SPH is very well suited for three-dimensional astrophysical problems that do not crucially rely on accurately resolved shock fronts.

Unlike other numerical approaches for hydrodynamics, the SPH equations do not take a unique form. Instead, many formally different versions of them can be derived. Furthermore, a large variety of recipes for specific implementations of force symmetrization, determinations of smoothing lengths, and artificial viscosity, have been described. Some of these choices are crucial for the accuracy and efficiency of the SPH implementation, others are only of minor importance. See the recent work by Thacker et al. (1998) and Lombardi et al. (1999) for a discussion of the relative performance of some of these possibilities. Below we give a summary of the specific SPH implementation we use. In it we have tried to combine some of the best formulations that have emerged, while simultaneously emphasizing accuracy and the need that the scheme must be amenable to an individual timestep integrator.

4.1. Basic equations

The computation of the hydrodynamic force and the rate of change of internal energy proceeds in two phases. In the first phase, new smoothing lengths h_i are determined for the *active* particles (these are the ones that need a force update at the current timestep, see below), and for each of them, the neighbouring particles inside their respective smoothing radii are found. The Lagrangian nature of SPH arises when this number of neighbours is kept either exactly, or at least roughly, constant. This is achieved by varying the smoothing length of each particle accordingly. The h_i thus adjust to the local particle density adaptively, leading to a constant mass resolution independent of the density of the flow. Nelson & Papaloizou (1994) argue that it is actually best to keep the number of neighbours exactly constant, resulting in the lowest level of ‘noise’ in SPH estimates of fluid quantities, and in the best conservation of energy. In practice however, similarly good results are obtained if the fluctuations in neighbour number remain small. In the serial version of GADGET we keep the number of neighbours fixed, whereas it is allowed to vary in a small band in the parallel code.

Having found the neighbours, we compute the density of the active particles as

$$\rho_i = \sum_{j=1}^N m_j W(\mathbf{r}_{ij}; h_i), \quad (22)$$

where $\mathbf{r}_{ij} \equiv \mathbf{r}_i - \mathbf{r}_j$, and we compute a new estimate of

divergence and vorticity as

$$\rho_i(\nabla \cdot \mathbf{v})_i = \sum_j m_j (\mathbf{v}_j - \mathbf{v}_i) \nabla_i W(\mathbf{r}_{ij}; h_i), \quad (23)$$

$$\rho_i(\nabla \times \mathbf{v})_i = \sum_j m_j (\mathbf{v}_i - \mathbf{v}_j) \times \nabla_i W(\mathbf{r}_{ij}; h_i). \quad (24)$$

Here we employ the *gather* formulation for adaptive smoothing (Hernquist & Katz, 1989).

For the *passive* particles, values for density, internal energy, and smoothing length are predicted at the current time based on the values of the last update of those particles (see Section 5). Finally, the pressure of the particles is set to $P_i = (\gamma - 1)\rho_i u_i$.

In the second phase, the actual forces are computed. Here we symmetrize the kernels of *gather* and *scatter* formulations as in Hernquist & Katz (1989). We compute the gasdynamical accelerations as

$$\mathbf{a}_i^{\text{gas}} = - \left(\frac{\nabla P}{\rho} \right)_i + \mathbf{a}_i^{\text{visc}} = - \sum_j m_j \left(\frac{P_i}{\rho_i^2} + \frac{P_j}{\rho_j^2} + \tilde{\Pi}_{ij} \right) \left[\frac{1}{2} \nabla_i W(\mathbf{r}_{ij}; h_i) + \frac{1}{2} \nabla_i W(\mathbf{r}_{ij}; h_j) \right], \quad (25)$$

and the change of the internal energy as

$$\frac{du_i}{dt} = \frac{1}{2} \sum_j m_j \left(\frac{P_i}{\rho_i^2} + \frac{P_j}{\rho_j^2} + \tilde{\Pi}_{ij} \right) (\mathbf{v}_i - \mathbf{v}_j) \left[\frac{1}{2} \nabla_i W(\mathbf{r}_{ij}; h_i) + \frac{1}{2} \nabla_i W(\mathbf{r}_{ij}; h_j) \right]. \quad (26)$$

The artificial viscosity $\tilde{\Pi}_{ij}$ is taken to be

$$\tilde{\Pi}_{ij} = \frac{1}{2} (f_i + f_j) \Pi_{ij}, \quad (27)$$

with

$$\Pi_{ij} = \begin{cases} [-\alpha c_{ij} \mu_{ij} + 2\alpha \mu_{ij}^2] / \rho_{ij} & \text{if } \mathbf{v}_{ij} \cdot \mathbf{r}_{ij} < 0 \\ 0 & \text{otherwise,} \end{cases} \quad (28)$$

where

$$f_i = \frac{|(\nabla \cdot \mathbf{v})_i|}{|(\nabla \cdot \mathbf{v})_i| + |(\nabla \times \mathbf{v})_i|}, \quad (29)$$

and

$$\mu_{ij} = \frac{h_{ij} (\mathbf{v}_i - \mathbf{v}_j) (\mathbf{r}_i - \mathbf{r}_j)}{|\mathbf{r}_i - \mathbf{r}_j|^2 + \epsilon h_{ij}^2}. \quad (30)$$

This form of artificial viscosity is the shear-reduced version (Balsara, 1995; Steinmetz, 1996) of the ‘standard’ Monaghan & Gingold (1983) artificial viscosity. Recent studies (Lombardi et al., 1999; Thacker et al., 1998) that test SPH implementations strongly endorse it.

In equations (25) and (26), a given SPH particle i will interact with a particle j whenever $|\mathbf{r}_{ij}| < h_i$ or $|\mathbf{r}_{ij}| < h_j$.

Standard search techniques can easily find all neighbours of particle i inside a sphere of radius h_i , but making sure that one really finds all interacting pairs in the case $h_j > h_i$ is more tricky. One solution to this problem is to simply find all neighbours of i inside h_i , and to consider the force components

$$\mathbf{f}_{ij} = -m_i m_j \left(\frac{P_i}{\rho_i^2} + \frac{P_j}{\rho_j^2} + \tilde{\Pi}_{ij} \right) \frac{1}{2} \nabla_i W(\mathbf{r}_{ij}; h_i). \quad (31)$$

If we add \mathbf{f}_{ij} to the force on i , and $-\mathbf{f}_{ij}$ to the force on j , the sum of equation (25) is reproduced, and the momentum conservation is manifest. This also holds for the internal energy. Unfortunately, this only works if all particles are active. For our individual timestep scheme, we therefore need an efficient way to find all the neighbours of particle i in the above sense, and we discuss our algorithm for doing this below.

4.2. Neighbour search

In SPH, a basic task is to find the nearest neighbours of each SPH particle to construct its interaction list. Specifically, one needs to find all particles closer than a search radius h_i in order to estimate the density, and one needs all particles with $|\mathbf{r}_{ij}| < \max(h_i, h_j)$ for the estimation of hydrodynamical forces. Similar to gravity, the naive solution that checks the distance of *all* particle pairs is an $\mathcal{O}(N^2)$ algorithm which slows down prohibitively for large particle numbers. Fortunately, there are faster search algorithms.

When the particle distribution is approximately homogeneous, perhaps the fastest algorithm works with a search grid that has a cell size equal to the search radius. The particles are then first coarse-binned on this search grid, and link-lists are established that quickly deliver only those particles that lie in a specific cell of the coarse grid. The neighbour search proceeds then by *range searching*; only those mesh cells have to be opened that have a spatial overlap with the search range.

For highly clustered particle distributions and varying search ranges h_i , the above approach quickly degrades, since the mesh chosen for the coarse grid has not the optimum size for all particles. A more flexible alternative is to employ a geometric search tree. For this purpose, a tree with a structure just like the BH oct-tree can be employed, and GADGET makes indeed use of the gravity tree of the SPH particles for this purpose. A neighbour search is then performed by walking the tree. A cell is ‘opened’ (i.e. further followed) if it has a spatial overlap with the rectangular search range. Note that testing for such an overlap is much faster with a rectangular search range than with a spherical one, so we inscribe the spherical search region into a little cube for the purpose of this walk. If one arrives at a cell with only one particle, this is added to the interaction list if it lies inside the search radius.

In the algorithm just described, the tree needs to be walked down all the way to the leaves containing the particles that

are going to end up in the interaction list. If the length of this tree walk can be reduced, the speed of the algorithm can be increased. In GADGET we use an additional trick to achieve this. A tree walk along a branch is terminated, if the cell lies *completely* inside the search range. Then all the particles in the cell can be added to the interaction list. But how can these particles be found in the first place without further walking the tree? It turns out that it is possible to set-up a link-list during the tree construction that allows a retrieval of all the particles that lie inside a given cell, just as it is done in the coarse-binning approach. This trick speeds up the neighbour search by a significant factor. Note that the ability to retrieve all particles in a given internal node of the tree is also used in our tree construction, and it is needed in our scheme to dynamically update parts of the tree, as will be described later on.

With a slight modification of the tree walk, we can also find all particles with $|\mathbf{r}_{ij}| < \max(h_i, h_j)$. For this purpose, we store in each tree node the maximum SPH smoothing length occurring among its particles. The test for overlap is then simply done between a cube of side-length $\max(h_i, h_{\text{node}})$ centered on the particle i and the node itself, where h_{node} is the maximum smoothing length among the particles of the node.

There remains the task to keep the number of neighbours around a given SPH particle approximately (or exactly) constant. We solve this by predicting a value \tilde{h}_i for the smoothing length based on the length h_i of the previous timestep, the actual number of neighbours N_i at that timestep, and the local velocity divergence:

$$\tilde{h}_i = \frac{1}{2} h_i^{(\text{old})} \left[1 + \left(\frac{N_s}{N_i} \right)^{1/3} \right] + \dot{h}_i \Delta t, \quad (32)$$

where $\dot{h}_i = \frac{1}{3} h_i (\nabla \cdot \mathbf{v})_i$, and N_s is the desired number of neighbours. The term in brackets tries to bring the number of neighbours back to the desired value, if N_i deviates from it. Should the resulting number of neighbours nevertheless fall outside a prescribed range of tolerance, we iteratively adjust h_i until the number of neighbours is again brought back to the desired range. Optionally, our code allows to impose a minimum smoothing length for SPH, typically chosen as some fraction of the gravitational softening length. More smoothing neighbours than N_s are allowed to occur if h_i takes on this minimum value.

One may also decide to keep the number of neighbours exactly constant by defining h_i to be the distance to the N_s -nearest particle. We employ such a scheme in our serial code. Here we carry out a range-search with $R = 1.2\tilde{h}_i$, on average resulting in $\sim 2N_s$ potential neighbours. From these we select the closest N_s (fast algorithms for doing this exist, see Press et al., 1995). If there are fewer than N_s particles in the search range, or if the distance of the N_s -nearest particle inside the search range is larger than R , the search is repeated for a larger search range. In the first timestep no previous h_i

is known, so we follow the neighbour tree backwards from the leave of the particle under consideration, until we obtain a first reasonable guess for the local particle density (based on the number N of particles in a node of volume l^3). This provides an initial guess for \tilde{h}_i .

However, the above scheme for keeping the number of neighbours exactly fixed is not easily accommodated in our parallel SPH implementation, because SPH particles may have a search radius that overlaps with several processor domains. In this case, the selection of the closest N_s neighbours becomes non-trivial, because the underlying data is distributed across several independent processor elements. For parallel SPH, we will therefore revert to the simpler scheme and allow the number of neighbours to fluctuate within a small band.

5. Time integration

As a time integrator, we use a variant of the leapfrog involving an explicit prediction step. The latter is introduced to accommodate individual particle timesteps in the N-body scheme, as explained later on.

We here start by describing the integrator for a single particle. First, a particle position at the middle of the timestep Δt is predicted according to

$$\tilde{\mathbf{r}}^{(n+\frac{1}{2})} = \mathbf{r}^{(n)} + \mathbf{v}^{(n)} \frac{\Delta t}{2}, \quad (33)$$

and an acceleration based on this position is computed, viz.

$$\mathbf{a}^{(n+\frac{1}{2})} = -\nabla\Phi|_{\tilde{\mathbf{r}}^{(n+\frac{1}{2})}}. \quad (34)$$

Then the particle is advanced according to

$$\mathbf{v}^{(n+1)} = \mathbf{v}^{(n)} + \mathbf{a}^{(n+\frac{1}{2})} \Delta t, \quad (35)$$

$$\mathbf{r}^{(n+1)} = \mathbf{r}^{(n)} + \frac{1}{2} [\mathbf{v}^{(n)} + \mathbf{v}^{(n+1)}] \Delta t. \quad (36)$$

5.1. Timestep criterion

In the above scheme, the timestep may vary from step to step. Note that the choice of timestep criterion is very important in determining the overall accuracy and computational efficiency of the integration.

In a static potential Φ , the error in specific energy arising in one step with the above integrator is

$$\begin{aligned} \Delta E &= \frac{1}{4} \frac{\partial^2 \Phi}{\partial x_i \partial x_j} v_i^{(n)} a_j^{(n+\frac{1}{2})} \Delta t^3 + \\ &\quad \frac{1}{24} \frac{\partial^3 \Phi}{\partial x_i \partial x_j \partial x_k} v_i^{(n)} v_j^{(n)} v_k^{(n)} \Delta t^3 + \mathcal{O}(\Delta t^4) \end{aligned} \quad (37)$$

to leading order in Δt , i.e. the integrator is second order accurate. Here the derivatives of the potential are taken at coordinate $\mathbf{r}^{(n)}$ and summation over repeated coordinate indices is understood.

In principle, one could try to use equation (38) directly to obtain a timestep by imposing some upper limit on the tolerable error ΔE . However, this approach is quite subtle in practice. First, the derivatives of the potential are difficult to obtain, and second, there is no explicit guarantee that the terms of higher order in Δt are really small.

To guarantee that the higher order terms indeed become smaller, one may consider the change of basic phase-space variables describing the particle. For example, the change of the position of the particle is

$$\Delta \mathbf{r} = \mathbf{r}^{(n+1)} - \mathbf{r}^{(n)} = \mathbf{v}^{(n)} \Delta t + \frac{1}{2} \mathbf{a}^{(n+\frac{1}{2})} \Delta t^2, \quad (38)$$

and its change in specific kinetic energy is

$$\Delta E_{\text{kin}} = \mathbf{v}^{(n)} \mathbf{a}^{(n+\frac{1}{2})} \Delta t + \frac{1}{2} \mathbf{a}^{(n+\frac{1}{2})} \mathbf{a}^{(n+\frac{1}{2})} \Delta t^2. \quad (39)$$

For a stable integration, the terms of second order in Δt should be smaller than the first order terms. This suggests a timestep criterion of the form

$$\Delta t = \alpha_{\text{tol}} \frac{|\mathbf{v}|}{|\mathbf{a}|}, \quad (40)$$

where α_{tol} is some dimensionless tolerance parameter. However, a well known problem of adaptive timestep schemes is that they usually break the time reversibility and symplectic nature of the simple leapfrog. As a result the system does not evolve under a pseudo-Hamiltonian any more, and secular drifts in the total energy can occur. A timestep criterion of the form (40) quite strongly breaks the reversibility of the integration, furthermore it is not Galilean invariant. As Quinn et al. (1997) show, reversibility can be resurrected with a timestep that depends only on the relative coordinates of particles. While our integration scheme is not reversible in the same way as theirs, it comes close to it when we choose to constrain the absolute size of the second order displacement of the kinetic energy by assuming a typical velocity dispersion σ^2 for the particles, corresponding to a scale $E = \sigma^2$ for the typical specific energy. This results in

$$\Delta t = \alpha_{\text{tol}} \frac{\sigma}{|\mathbf{a}|}. \quad (41)$$

Alternatively, we can constrain the second order term in the particle displacement, obtaining

$$\Delta t = \sqrt{\frac{2\alpha'_{\text{tol}} \epsilon}{|\mathbf{a}|}}. \quad (42)$$

Here some length scale $\alpha'_{\text{tol}} \epsilon$ is introduced, which will typically be related to the gravitational softening. We have found the criterion (41) to give the best results compared to several alternative choices, including (42). We will later show test calculations illustrating this in more detail.

The quantity $\alpha_{\text{tol}}\sigma$ controls the accuracy of the collisionless time integration. Our typical choice for simulations of interacting galaxies is of order $\alpha_{\text{tol}}\sigma \simeq 10-20$ km/sec. Note that the timestep criterion (41) is Galilean-invariant and does not make an explicit reference to the gravitational softening length employed.

5.2. Integrator for N-body systems

In contrast to a binary hierarchy of timesteps (Hernquist & Katz, 1989; Steinmetz, 1996), we employ an integrator with completely flexible timesteps, similar to the one employed by Groom (1997) and Hiotelis & Voglis (1991). Each particle owns a timestep Δt_i , and a current time t_i , where its dynamical state (\mathbf{r}_i , \mathbf{v}_i , \mathbf{a}_i) is stored. The dynamical state of the particle can be predicted at times $t \in [t_i \pm 0.5\Delta t_i]$ with first order accuracy.

The next particle k to be advanced is then the one with the minimum prediction time defined as $\tau_p \equiv \min(t_i + 0.5\Delta t_i)$. The time τ_p becomes the new current time of the system. To advance the corresponding particle, we first predict positions for *all* particles at time τ_p according to

$$\tilde{\mathbf{r}}_i = \mathbf{r}_i + \mathbf{v}_i(\tau_p - t_i). \quad (43)$$

Based on these positions, the acceleration of particle k at the middle of its timestep is calculated as

$$\mathbf{a}_k^{(n+\frac{1}{2})} = -\nabla\Phi(\tilde{\mathbf{r}}_i)|_{\tilde{\mathbf{r}}_k}. \quad (44)$$

Position and velocity of particle k are then advanced as

$$\mathbf{v}_k^{(n+1)} = \mathbf{v}_k^{(n)} + 2\mathbf{a}_k^{(n+\frac{1}{2})}(\tau_p - t_k), \quad (45)$$

$$\mathbf{r}_k^{(n+1)} = \mathbf{r}_k^{(n)} + \left[\mathbf{v}_k^{(n)} + \mathbf{v}_k^{(n+1)} \right] (\tau_p - t_k), \quad (46)$$

and its current time can be updated to

$$t_k^{(\text{new})} = t_k + 2(\tau_p - t_k). \quad (47)$$

Finally, a new timestep $\Delta t_k^{(\text{new})}$ for the particle is estimated.

At the beginning of the simulation, all particles start out with the same current time. However, since the timesteps of the particles are all different, the current times of the particles distribute themselves nearly symmetrically around the current prediction time, hence the prediction step involves forward and backward prediction to a similar extent.

Of course, it is impractical to advance only a single particle at any given prediction time, because the prediction itself and the (dynamic) tree updates induce some overhead. For this reason we advance particles in bunches. The particles may be thought of as being ordered according to their prediction times $t_i^p = t_i + \frac{1}{2}\Delta t_i$. The simulation works through this time line, and always advances the particle with the smallest

t_i^p , and also all subsequent particles in the time line, until the first is found with

$$\tau_p \leq t_i + \frac{1}{4}\Delta t_i. \quad (48)$$

This condition selects a group of particles at the lower end of the time line, and all the particles of the group are guaranteed to be advanced at least by half of their maximum allowed timestep.

Our practical experience shows that the size M of the group that is advanced at a given step is often only a small fraction of the total particle number N . In this situation it becomes important to eliminate any overhead that scales with $\mathcal{O}(N)$. For example, we obviously need to find the particle with the minimum prediction time at every timestep, and also the particles following it in the time line. A loop over all the particles, or a complete sort at every timestep, would induce overhead of order $\mathcal{O}(N)$ or $\mathcal{O}(N \log N)$, which can become comparable to the force computation itself if $M/N \ll 1$. We solve this problem by keeping the maximum prediction times of the particles in an ordered binary tree (Wirth, 1986) at all times. Finding the particle with the minimum prediction time and the ones that follow it are then operations of order $\mathcal{O}(\log N)$. Also, once the particles have been advanced, they can be removed and reinserted into this tree with a cost of order $\mathcal{O}(\log N)$. Together with the dynamic tree updates, which eliminate prediction and tree construction overhead, the cost of the timestep then scales as $\mathcal{O}(M \log N)$.

5.3. Dynamic tree updates

If the fraction of particles to be advanced at a given timestep is indeed small, the prediction of *all* particles and the reconstruction of the *full* tree would also lead to significant sources of overhead. However, the geometric structure of the tree, i.e. the way the particles are grouped into a hierarchy, evolves only relatively slowly in time. It is therefore sufficient to reconstruct this grouping only every few timesteps, provided one can still obtain accurate node properties (center of mass, multipole moments) at the current prediction time.

We achieve this by predicting properties of tree-nodes on the fly, instead of predicting *all* particles every single timestep. In order to do this, each node carries a center-of-mass velocity in addition to its position at the time of its construction. New node positions can then be predicted while the tree is walked, and only nodes that are actually visited need to be predicted. Note that the leaves of the tree point to single particles. If they are used in the force computation, their prediction corresponds exactly to the ordinary prediction as outlined in equation (46).

In our scheme we neglect a possible time variation of the quadrupole moment of the nodes. However, we have introduced an additional mechanism that reacts to fast time variations of tree nodes. Whenever the center-of mass of a tree

node under consideration has moved by more than a small fraction of the nodes' side-length since the last reconstruction of this part of the tree, the node is completely updated, i.e. the center-of-mass, center-of-mass velocity and quadrupole moment are recomputed from the individual (predicted) phase-space variables of the particles. We also adjust the side-length of the tree node if any of its particles should have left its original cubical volume.

Finally, the full tree is reconstructed from scratch every once in a while to take into account the slow changes in the grouping hierarchy. Typically we update the tree whenever a total of $\sim 0.1N$ force computations have been done since the last full reconstruction. With this criterion the tree construction is only an insignificant fraction of the total computation time, while we have not noticed any significant loss of force accuracy induced by this procedure.

In summary, the algorithms described above result in an integration scheme that can smoothly and efficiently evolve an N-body system containing a very large dynamic range in time scales. At a given timestep, only a small number M of particles are then advanced, and the total time required for that scales as $\mathcal{O}(M \log N)$.

5.4. Including SPH

The above time integration scheme may easily be extended to include SPH. Here we also need to integrate the internal energy equation, and the particle accelerations also receive a hydrodynamical component. To compute the latter we also need predicted velocities

$$\tilde{\mathbf{v}}_i = \mathbf{v}_i + \mathbf{a}_{i-1}(\tau_p - t_i), \quad (49)$$

where we have approximated \mathbf{a}_i with the acceleration of the previous timestep. Similarly, we obtain predictions for the internal energy

$$\tilde{u}_i = u_i + \dot{u}_i(\tau_p - t_i), \quad (50)$$

and the density of *inactive* particles as

$$\tilde{\rho}_i = \rho_i + \dot{\rho}_i(\tau_p - t_i). \quad (51)$$

For those particles that are to be advanced at the current system step, these predicted quantities are then used to compute the hydrodynamical part of the acceleration and the rate of change of the internal energy with the usual SPH estimates, as described in Section 4.

Note that the timestep criterion (41) needs to be supplemented with the Courant condition for the gas particles. We adopt it in the form

$$\Delta t_i = \frac{\alpha_{\text{cour}} h_i}{h_i |(\nabla \cdot \mathbf{v})_i| + \max(c_i, |\mathbf{v}_i|) (1 + 0.6 \alpha_{\text{visc}})}, \quad (52)$$

where α_{visc} regulates the strength of the artificial bulk viscosity, and α_{cour} is an accuracy parameter, the Courant factor. Note that we use the maximum of the sound speed c_i and

the bulk velocity $|\mathbf{v}_i|$ in this expression. This improves the handling of strong shocks when the infalling material is cold. For the SPH-particles, we use either criterion (41) or (52), whichever gives the smaller timestep.

As defined above, we evaluate \mathbf{a}^{gas} and \dot{u} at the middle of the timestep, when the actual timestep Δt of the particle that will be advanced is *already set*. Note that there is a term in the artificial viscosity that can cause a problem in this explicit integration scheme. The second term in equation (28) tries to prevent particle inter-penetration. If a particle happens to get relatively close to another SPH particle in the time $\Delta t/2$ and the relative velocity of the approach is large, this term can suddenly lead to a very large repulsive acceleration \mathbf{a}^{visc} trying to prevent the particles from getting any closer. However, it is then too late to reduce the timestep. Instead, the velocity of the approaching particle will be changed by $\mathbf{a}^{\text{visc}} \Delta t$, possibly *reversing* the approach of the two particles. But the artificial viscosity should at most *halt* the approach of the particles. To guarantee this, we introduce an upper cut-off to the maximum acceleration induced by the artificial viscosity. If $\mathbf{v}_{ij} \cdot \mathbf{r}_{ij} < 0$, we replace equation (27) with

$$\tilde{\Pi}_{ij} = \frac{1}{2}(f_i + f_j) \min \left[\Pi_{ij}, \frac{\mathbf{v}_{ij} \cdot \mathbf{r}_{ij}}{(m_i + m_j)W_{ij}\Delta t} \right], \quad (53)$$

where $W_{ij} = \mathbf{r}_{ij} \nabla_i [W(\mathbf{r}_{ij}; h_i) + W(\mathbf{r}_{ij}; h_j)]/2$. With this change, the integration scheme works still reasonably well in regimes with strong shocks under conditions of relatively coarse timestepping. Of course, a small enough value of the Courant factor will prevent this situation from occurring to begin with.

Since we use the gravitational tree of the SPH particles for the neighbour search, another subtlety arises in the context of dynamic tree updates, where the full tree is not necessarily reconstructed every single timesteps. Note that our range searching technique relies on the *current* values of the maximum SPH smoothing length in each node, and also expects that all particles of a node still are inside the boundaries set by the side-length of a node. To guarantee that the neighbour search will always give correct results, we therefore perform a special update of the SPH-tree every timestep. It involves visiting every node and updating its maximum h_i and side-length accordingly. By using the link-list structure of every node to access its particles, the overhead incurred by this is kept very small.

5.5. Implementation of cooling

When radiative cooling is included in simulations of galaxy formation or galaxy interaction, additional numerical problems arise. In regions of strong gas cooling, the cooling times can become so short, that extremely small timesteps would be required to follow the internal energy accurately with the simple explicit scheme used so far.

To remedy this problem, we treat the cooling semi-implicitly in an isochoric approximation. At any given timestep, we first compute the rate \dot{u}^{ad} of change of the internal energy due to the ordinary adiabatic gas physics. In an isochoric approximation, we then solve implicitly for a new internal energy predicted at the end of the timestep, i.e.

$$\hat{u}_i^{(n+1)} = u_i^{(n)} + \dot{u}^{\text{ad}} \Delta t - \frac{\Lambda \left[\rho_i^{(n)}, \hat{u}_i^{(n+1)} \right] \Delta t}{\rho_i^{(n)}}. \quad (54)$$

The implicit computation of the cooling rate guarantees stability. Based on this estimate, we compute an effective rate of change of the internal energy, which we then take as

$$\dot{u}_i = \left[\hat{u}_i^{(n+1)} - u_i^{(n)} \right] / \Delta t. \quad (55)$$

This last step is necessary since our integration scheme requires the possibility to predict the internal energy at arbitrary times. With the above procedure, u_i is always a continuous function of time, and the prediction of u_i may be done for times in between the application of the isochoric cooling/heating.

5.6. Integration in comoving coordinates

For simulations in a cosmological context, the expansion of the universe has to be taken into account. Let \mathbf{x} denote comoving coordinates, and a be the dimensionless scale factor ($a = 1.0$ at the present epoch). Then the Newtonian equation of motion becomes

$$\ddot{\mathbf{x}} + 2\frac{\dot{a}}{a} \dot{\mathbf{x}} = -G \int \frac{\delta\rho(\mathbf{x}') (\mathbf{x} - \mathbf{x}')}{|\mathbf{x} - \mathbf{x}'|^3} d^3x'. \quad (56)$$

Here the function $\delta\rho(\mathbf{x}) = \rho(\mathbf{x}) - \bar{\rho}$ denotes the (proper) density fluctuation field.

In an N-body simulation with periodic boundary conditions, the volume integral of equation (56) is carried out over *all* space. As a consequence, the homogeneous contribution arising from $\bar{\rho}$ drops out around every point. Then the equation of motion of particle i becomes

$$\ddot{\mathbf{x}}_i + 2\frac{\dot{a}}{a} \dot{\mathbf{x}}_i = -\frac{G}{a^3} \sum_{\substack{j \neq i \\ \text{periodic}}} \frac{m_j (\mathbf{x}_i - \mathbf{x}_j)}{|\mathbf{x}_i - \mathbf{x}_j|^3}, \quad (57)$$

where the summation includes all periodic images of the particles j .

However, one may also employ vacuum boundary conditions. Here, one simulates a spherical region of radius R around the origin, and neglects density fluctuations outside this region. In this case, the background density $\bar{\rho}$ gives rise to an additional term, viz.

$$\ddot{\mathbf{x}}_i + 2\frac{\dot{a}}{a} \dot{\mathbf{x}}_i = \frac{1}{a^3} \left[-G \sum_{j \neq i} \frac{m_j \mathbf{x}_{ij}}{|\mathbf{x}_{ij}|^3} + \frac{1}{2} \Omega_0 H_0^2 \mathbf{x}_i \right]. \quad (58)$$

GADGET supports both periodic and vacuum boundary conditions. We implement the former by means of the Ewald summation technique (Hernquist et al., 1991).

For this purpose, we modify the tree walk such that each node is mapped to the position of its nearest periodic image with respect to the coordinate under consideration. If the multipole expansion of the node can be used according to the cell opening criterion, its partial force is computed in the usual way. However, we also need to add the force exerted by all the other periodic images of the node. The slowly converging sum over these contributions can be evaluated with the Ewald technique. If \mathbf{x} is the coordinate of the point of force-evaluation relative to a node of mass M , the resulting *additional* acceleration is given by

$$\mathbf{a}_c(\mathbf{x}) = M \left\{ \frac{\mathbf{x}}{|\mathbf{x}|^3} - \sum_{\mathbf{n}} \frac{\mathbf{x} - \mathbf{n}L}{|\mathbf{x} - \mathbf{n}L|^3} \times \left[\text{erfc}(\alpha|\mathbf{x} - \mathbf{n}L|) + \frac{2\alpha|\mathbf{x} - \mathbf{n}L|}{\sqrt{\pi}} \exp(-\alpha^2|\mathbf{x} - \mathbf{n}L|^2) \right] - \frac{2}{L^2} \sum_{\mathbf{h} \neq 0} \frac{\mathbf{h}}{|\mathbf{h}|^2} \exp\left(-\frac{\pi^2|\mathbf{h}|^2}{\alpha^2 L^2}\right) \sin\left(\frac{2\pi}{L} \mathbf{h} \cdot \mathbf{x}\right) \right\}. \quad (59)$$

Here \mathbf{n} and \mathbf{h} are integer triplets, L is the box size, and α is an arbitrary number (Hernquist et al., 1991). Good convergence is achieved for $\alpha = 2/L$, where we sum over the range $|\mathbf{n}| < 5$ and $|\mathbf{h}| < 5$. Similarly, the additional potential due to the periodic replications of the node is given by

$$\phi_c(\mathbf{x}) = M \left\{ \frac{1}{\mathbf{x}} + \frac{\pi}{\alpha^2 L^3} - \sum_{\mathbf{n}} \frac{\text{erfc}(\alpha|\mathbf{x} - \mathbf{n}L|)}{|\mathbf{x} - \mathbf{n}L|} - \frac{1}{L} \sum_{\mathbf{h} \neq 0} \frac{1}{\pi|\mathbf{h}|^2} \exp\left(-\frac{\pi^2|\mathbf{h}|^2}{\alpha^2 L^2}\right) \cos\left(\frac{2\pi}{L} \mathbf{h} \cdot \mathbf{x}\right) \right\}. \quad (60)$$

We follow Hernquist et al. (1991) and tabulate the correction fields $\mathbf{a}_c(\mathbf{x})/M$ and $\phi_c(\mathbf{x})/M$ for one octant of the simulation box, and obtain the result of the Ewald summation during the tree walk from trilinear interpolation off this grid. It should be noted however, that periodic boundaries have a strong impact on the speed of the tree algorithm. The number of floating point operations required to interpolate the correction forces from the grid have a significant toll on the raw force speed.

In linear theory, it can be shown that the kinetic energy

$$T = \frac{1}{2} \sum_i m_i \mathbf{v}^2 \quad (61)$$

in peculiar motion grows proportional to a , at least at early times. This implies that $\sum_i m_i \dot{\mathbf{x}}^2 \propto 1/a$, hence the comoving velocities $\dot{\mathbf{x}} = \mathbf{v}/a$ actually diverge for $a \rightarrow 0$. Since cosmological simulations are usually started at redshift $z \simeq 30 - 100$, one therefore needs to follow a rapid deceleration of $\dot{\mathbf{x}}$ at high redshift. So it is numerically unfavourable to solve the equations of motion in the variable $\dot{\mathbf{x}}$.

To remedy this problem, we use an alternative velocity variable

$$\mathbf{w} \equiv a^{\frac{1}{2}} \dot{\mathbf{x}}, \quad (62)$$

and we employ the expansion factor itself as time variable. Then the equations of motion become

$$\frac{d\mathbf{w}}{da} = -\frac{3}{2} \frac{\mathbf{w}}{a} + \frac{1}{a^2 S(a)} \left[-G \sum_{j \neq i} \frac{m_j \mathbf{x}_{ij}}{|\mathbf{x}_{ij}|^3} + \frac{1}{2} \Omega_0 H_0^2 \mathbf{x}_i \right], \quad (63)$$

$$\frac{d\mathbf{x}}{da} = \frac{\mathbf{w}}{S(a)}, \quad (64)$$

with $S(a) = a^{\frac{3}{2}} H(a)$ given by

$$S(a) = H_0 \sqrt{\Omega_0 + a(1 - \Omega_0 - \Omega_\Lambda) + a^3 \Omega_\Lambda}. \quad (65)$$

Note that for periodic boundaries the second term in the square bracket of equation (63) is absent, instead the summation extends over all periodic images of the particles.

Using the Zel'dovich approximation, one sees that \mathbf{w} remains constant in the linear regime. Strictly speaking this holds only for an Einstein-de-Sitter universe at all times, however, it is also true for other cosmologies at early times. Hence equations (62) to (65) in principle solve linear theory for arbitrarily large steps in a . This allows to traverse the linear regime with maximum computational efficiency. Furthermore, equations (62) to (65) represent a convenient formulation for general cosmologies, and for our variable timestep integrator. Since \mathbf{w} does not vary in the linear regime, predicted particle positions based on $\tilde{\mathbf{x}}_i = \mathbf{x}_i + \mathbf{w}_i (a_p - a_i) / S(a_p)$ are quite accurate. Also, the acceleration entering the timestep criterion may now be identified with $d\mathbf{w}/da$, and the timestep becomes

$$\Delta a = \alpha_{\text{tol}} \sigma \left| \frac{d\mathbf{w}}{da} \right|^{-1}. \quad (66)$$

The above equations only treated the gravity part of the dynamical equations. However, it is straightforward to express the hydrodynamical equations in the variables (\mathbf{x} , \mathbf{w} , a) as well. For gas particles, equation (63) receives an additional contribution due to hydrodynamical forces, viz.

$$\left(\frac{d\mathbf{w}}{da} \right)_{\text{hydro}} = -\frac{1}{a S(a)} \frac{\nabla_{\mathbf{x}} P}{\rho}. \quad (67)$$

For the energy equation, one obtains

$$\frac{du}{da} = -\frac{3}{a} \frac{P}{\rho} - \frac{1}{S(a)} \frac{P}{\rho} \nabla_{\mathbf{x}} \cdot \mathbf{w}. \quad (68)$$

Here the first term on the right hand side describes the adiabatic cooling of gas due to the expansion of the universe.

6. Parallelization

Massively parallel computer systems with distributed memory have become increasingly popular recently. They can be thought of as a collection of workstations, connected by a fast communication network. This architecture promises large scalability for reasonable cost. Current state-of-the art machines of this type include Cray T3E and IBM SP/2. It is an interesting development that ‘Beowulf’-type systems based on commodity hardware have started to offer floating point performance comparable to these supercomputers, albeit at a much lower price.

However, an efficient use of parallel distributed memory machines often requires substantial changes of existing algorithms, or the development of completely new ones. Conceptually, parallel programming involves two major difficulties in addition to the task of solving the numerical problem in a serial code. First, there is the difficulty of how to divide the work and data *evenly* among the processors, and second, an efficient communication scheme between the processors needs to be devised.

In recent years, a number of groups have developed parallel N-body codes, all of them with different parallelization strategies, and different strengths and weaknesses. An early attempt for parallelization has been done by Theuns & Rathsack (1993). Later, Warren et al. (1992) parallelized the BH-tree code for the first time on massively parallel machines. Dubinski (1996) presented the first parallel tree code based on MPI. Dikaiakos & Stadel (1995) have developed a parallel simulation code (PKDGRAV) that works with a balanced binary tree. More recently, parallel tree-SPH codes have been introduced by Davé et al. (1997) and Lia & Carraro (1999), and a PVM implementation of a gravity-only tree code has been described by Viturro & Carpintero (2000).

We here report on our newly developed parallel version of GADGET, a tree-SPH code that differs in important ways from the parallelization strategy adopted by other workers. For the first time it implements individual particle timesteps for all particles in a massively parallel N-body code. We have used the *Message Passing Interface* (MPI) (Pacheco, 1997; Snir et al., 1995), which is an explicit communication scheme, i.e. it is entirely up to the user to control the communication. Messages containing data can be sent between processors, both in synchronous and asynchronous modes. A particular advantage of MPI is its flexibility and portability. Our simulation code uses only standard C and standard MPI, and should therefore run on a variety of platforms. We have confirmed this so far on Cray T3E and IBM SP/2 systems, and on Linux-PC clusters.

6.1. Domain decomposition

The typical size of problems attacked on parallel computers is usually much too large to fit into the memory of individ-

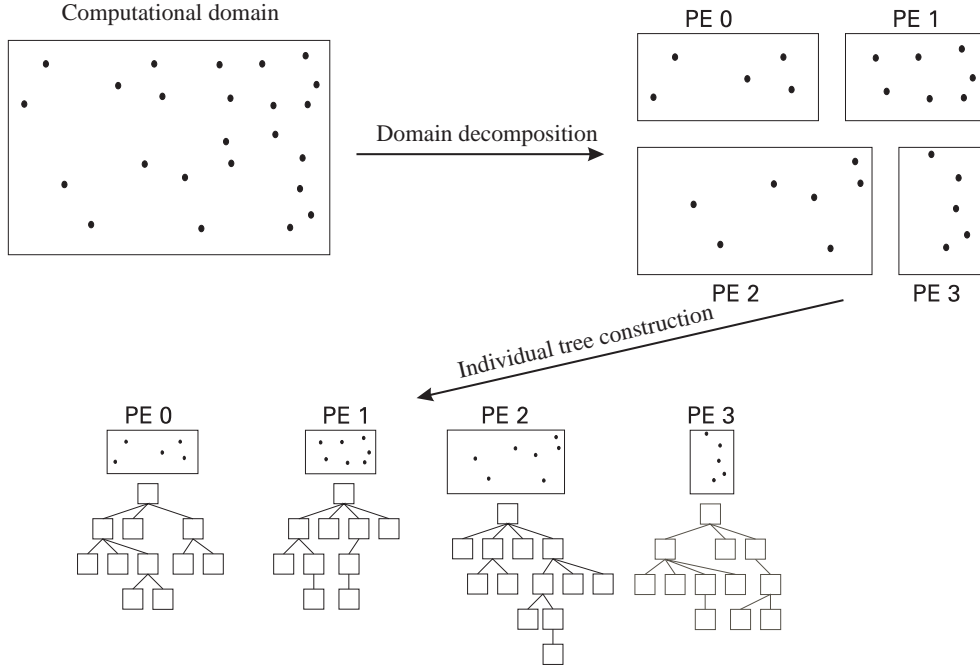


Figure 2: Schematic representation of the domain decomposition in two dimensions, and for four processors. Here, the first split occurs along the y-axis, separating the processors into two groups. They then independently carry out a second split along the x-axis. After completion of the domain decomposition, each processor element (PE) can construct its own BH tree just for the particles in its part of the computational domain.

ual computational nodes, or into ordinary workstations. This fact alone, but of course also the desire to distribute the work among the processors, requires a partitioning of the problem onto the individual processors.

For our N-body/SPH code we have implemented a spatial domain decomposition. The particular algorithm we use for the split is an orthogonal recursive bisection (ORB) (Dubinski, 1996). In the first step, a split is found along one spatial direction, e.g. the x-axis, and the collection of processors is grouped into two halves, one for each side of the split. These processors then exchange particles such that they end up hosting only particles lying on their side of the split. In the simplest possible approach, the position of the split is chosen such that there are an equal number of particles on both sides. However, for an efficient simulation code the split should try to balance the work done in the force computation on both sides. This aspect will be discussed further below.

In a second step, each group of processors finds a new split along a different spatial axis, e.g. the y-axis. This splitting process is repeated recursively until the final groups consist of just one processor, which then hosts a rectangular piece of the computational volume. Note that this algorithm constrains the number of processors that may be used to a power of two.

A two-dimensional schematic illustration of the ORB is shown in Figure 2. Note that each processor can construct a local BH tree for its domain, and this tree may be used to

compute the force exerted by the processors' particles on arbitrary test particles in space.

6.2. Parallel computation of the gravitational force

Our algorithm for parallel force computation differs significantly from that of Dubinski (1996). He uses the notion of *locally essential trees*. These are trees that are sufficiently detailed to allow the full force computation for any particle local to a processor, without further need for information from other processors. The locally essential trees can be constructed from the local trees by pruning and exporting parts of these trees to other processors, and attaching these parts as new branches to the local trees. To determine which parts of the trees need to be exported, special tree walks are required.

A disadvantage of this technique is that the construction of the locally essential trees is a complicated, time-consuming process that needs to be repeated every time-step. While this should not be an issue for an integration scheme with a global timestep, the tree construction time would dominate the computational time for our individual timestep scheme, where typically of order 1 per cent of all particles require a force update at one of the (small) system timesteps. Therefore we chose a different parallelization scheme that essentially scales linearly with the number of particles that need a force computation.

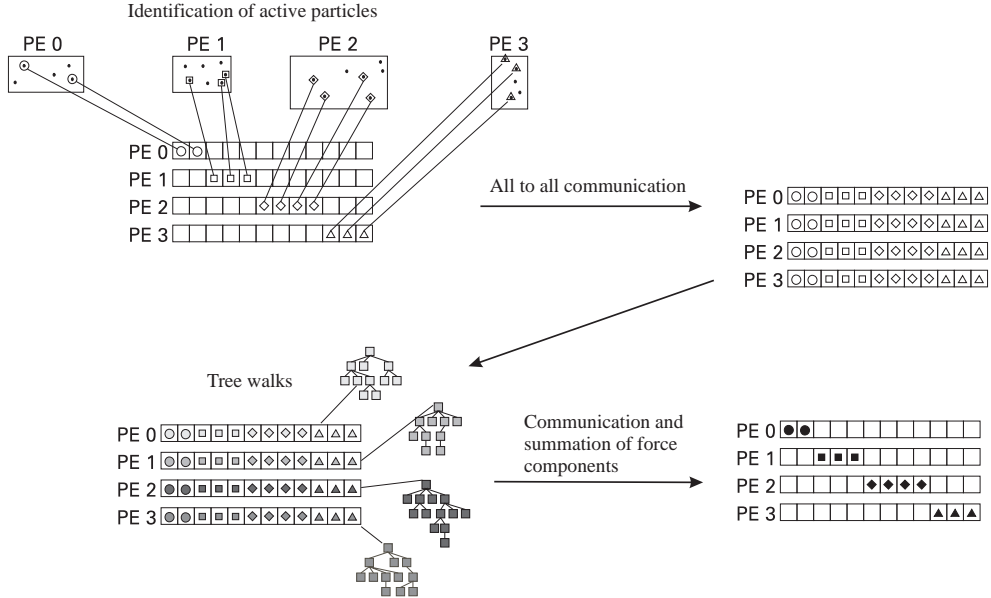


Figure 3: Schematic illustration of the parallelization scheme of GADGET for the force computation. In the first step, each PE identifies the active particles, and puts their coordinates in a communication buffer. In a communication phase, a single and identical list of all these coordinates is then established on all processors. Then each PE walks its local tree for this list, thereby obtaining a list of partial forces. These are then communicated in a collective process back to the original PE that hosts the corresponding particle coordinate. Each processor then sums up the incoming force contributions, and finally arrives at the required total forces for its active particles.

Our strategy starts from the observation that each of the local processor trees is able to provide the force exerted by its particles for any location in space. The full force might thus be obtained by adding up all the partial forces from the local trees. As long as the number of these trees is less than the number of typical particle-node interactions, this computational scheme is practically not more expansive than a tree walk of the corresponding locally essential tree.

A force computation therefore requires a communication of the desired coordinates to all processors. These then walk their local trees, and send partial force components back to the original processor that sent out the corresponding coordinate. The total force is then obtained by summing up the incoming contributions.

In practice, a force computation for a *single* particle would be badly imbalanced in work in such a scheme, since some of the processors could stop their tree walk already at the root node, while others would have to evaluate several hundred particle-node interactions. However, our time integration scheme advances at a given timestep always a group M of particles of size about 0.5–5 per cent of the total number of particles. This group represents a representative mix of the various clustering states of matter in the simulation. Each processor contributes some of its particle positions to this mix, but the total list of coordinates is the same *for all* processors. If the domain decomposition is done well, one can arrange that the cumulative time to walk the local tree for

all coordinates in this list is the same for all processors.

Our force computation scheme proceeds therefore as sketched schematically in Figure 3. Each processor identifies the particles that are to be advanced in the current timestep, and puts their coordinates in a communication buffer. Next, an all-to-all communication phase is used to establish the same list of coordinates on all processors. This communication is done in a collective fashion: For N_p processors, the communication involves $N_p - 1$ cycles. In each cycle, the processors are arranged in $N_p/2$ pairs. Each pair exchanges their original list of active coordinates. In this way, the communication is done fully in parallel, and the time it requires scales as $\mathcal{O}(MN_p)$. On the T3E, the communication bandwidth is large enough that only a very small fraction of the overall simulation time is spent in this phase, even if processor partitions as large as 512 are used.

In the next step, all processors walk their local trees and replace the coordinates with the corresponding force contribution. Note that this is the most time-consuming step of a collisionless simulation (as it should be), hence work-load balancing is most crucial here. After that, the force contributions are communicated in a similar way as above between the processor pairs. The processor that hosted a particular coordinate adds up the incoming force contributions and finally ends up with the full force for that location. These forces can then be used to advance its locally active particles, and to determine new timesteps for them. In these phases of the N-

body algorithm, as well as in the tree construction, no further information from other processors is required.

6.3. Work-load balancing

Due to the high communication bandwidth of parallel supercomputers like the T3E or the SP/2, the time required for force computation is dominated by the tree walks, and this is also the dominating part of the simulation as a whole. It is therefore crucial that this part of the computation parallelizes well. In the context of our parallelization scheme, this means that the domain decomposition should be done such that the time spent in the tree walks is the same for all processors.

It is helpful to note, that the list of coordinates for the tree walks is *independent* of the domain decomposition. We can then think of each patch of space, represented by its particles, to cause some cost in the tree-walk process. A good measure for this cost is the number of particle-node interactions originating from this region of space. To balance the work, the domain decomposition should therefore try to make this cost equal on both sides of each domain split.

In practice, we try to reach this goal by letting each tree-node carry a counter for the number of node-particle interactions it participated in since the last domain decomposition occurred. Before a new domain decomposition starts, we then assign this cost to individual particles in order to obtain a weight factor reflecting the cost they on average incur in the gravity computation. For this purpose, we have implemented a method to walk the tree backwards from a leaf (i.e. a single particle) to the root node. In this walk, the particle collects its total cost by adding up its share of the cost from all its parent nodes. In this respect, our work-load balancing scheme differs somewhat from that of Dubinski (1996).

Note that an optimum work-load balance often results in substantial memory imbalance. Tree-codes consume plenty of memory, so that the feasible problem size can become memory rather than CPU-time limited. For example, a single node with 128 Mbyte on the Garching T3E is already filled to roughly 65 per cent with 4.0×10^5 particles, including all memory for the tree structures, and the time integration scheme. In this example, the remaining free memory can already be insufficient to guarantee optimum work-load balancing in strongly clustered simulations. Unfortunately, such a situation is not untypical in practice, since one usually strives for *large N* in N-body work, so one is always tempted to fill up most of the available memory with particles, without leaving much room to balance the work-load. Of course, GADGET can only try to balance the work within the limits set by the available memory.

6.4. Parallelization of SPH

Hydrodynamics can be seen as a more natural candidate for parallelization than gravity, because it is a *local* interaction.

In contrast to this, the gravitational N-body problem has the nasty property that at all times *each particle interacts with every other particle*, making gravity intrinsically difficult to parallelize on distributed memory machines.

It therefore comes as no large surprise that the parallelization of SPH can be handled by invoking the same strategy we employed for the gravitational part, with only minor adjustments that take into account that most SPH particles (those entirely ‘inside’ a local domain) do not rely on information from other processors.

In particular, similar as in the purely gravitational case, we do not import neighbouring particles from other processors in order to allow a computation of the full SPH forces on the local processor. Rather, we export the particle coordinates (and other information, if needed) to other processors, which then deliver partial hydrodynamical forces or partial densities contributed by their particle population. For example, the density computation of SPH can be handled in much the same way as that of the gravitational forces. In a collective communication, the processors establish a common list of all coordinates of active particles together with their smoothing lengths. Each processor then computes partial densities by finding those of its particles that lie within each smoothing region, and by doing the usual kernel weighting for them. These partial densities are then delivered back to the processor that holds the particle corresponding to a certain entry in the list of active coordinates. This processor then adds up the partial contributions, and obtains the full density estimate for the active particle.

The locality of the SPH interactions brings an important simplification to this scheme. If the smoothing region of a particle lies entirely inside a local domain, the particle coordinate does not have to be exported at all, allowing a large reduction in the length of the common list of coordinates each processor has to work on, and – more importantly – reducing the necessary amount of communication involved dramatically.

In the first phase of the SPH computation, we compute in this way not only the density, but also the total number of neighbours inside the smoothing length, and we evaluate velocity divergence and curl. In the second phase, the hydrodynamical forces are then evaluated in an analogous fashion.

Notice that the computational cost and the communication overhead of this scheme again scale linearly with the number M of active particles, a feature that is essential for good adaptivity of the code. We also note that in the second phase of the SPH computation, the particles ‘see’ the updated density values automatically. When SPH particles themselves are imported, they have to be exchanged a second time if they are active particles themselves in order to have correctly updated density values for the hydrodynamical force computation.

An interesting complication arises when the domain decomposition is not repeated every timestep. In practice this means that the boundaries of a domain may become ‘diffuse’

when some particles start to move out of the boundaries of the original domain. If the spatial region that we classified as ‘interior’ of a domain is not adjusted, we then risk missing interactions because we might not export a particle that starts to interact with a particle that has entered the local domain boundaries, but is still hosted by another processor. Note that our method to update the neighbour-tree on each single timestep guarantees that always the correct neighbouring particles are found on a local processor - if such a search is conducted at all. So in the case of these soft domain boundaries we need to make sure that all particles really are exported that can possibly interact with particles on other processors.

We achieve this by ‘shrinking’ the interior of the local domain. During the neighbour-tree update, we find the maximum spatial extension of all SPH particles on the local domain. These rectangular regions are then gathered from all other processors, and cut with the local extension. If an overlap occurs the local ‘interior’ is reduced accordingly, thereby resulting in a region that is guaranteed not to contain any particle that lies on another processor. In this way, the SPH algorithm will always produce correct results, even if the domain decomposition is repeated only rarely, or never again. Note that in the case of periodic boundaries, special care has to be taken in treating cuts of the current interior with periodic translations of the other domain extensions.

7. Results and tests

7.1. Tests of timestep criteria

As first tests of the relative performance of different timestep criteria, we integrate a particle orbit in the potential of a point mass, and in the potential of an isothermal sphere. We consider three simple timestep criteria, which are based on the acceleration and/or velocity of the particle in the previous timestep. These criteria are

$$(A) \quad \Delta t = \frac{\eta_A}{|\mathbf{a}|}, \quad (69)$$

$$(B) \quad \Delta t = \frac{\eta_B}{\sqrt{|\mathbf{a}|}}, \quad (70)$$

$$(C) \quad \Delta t = \frac{\eta_C}{|\mathbf{v}| |\mathbf{a}|}. \quad (71)$$

Criterion (A) is the of form suggested in this work, while both (B) and (C) have been used in previous studies (among others: Quinn et al., 1997; Heller & Shlosman, 1994).

We now consider a test particle in the field of a point mass. We adjust the coefficients η_A , η_B , η_C of the timestep criteria such that they all integrate a circular orbit of given radius with $N = 50$ force computations. For the circular orbit, the timestep remains fixed, and the integration is symplectic for all three criteria, without any secular drift in energy. It is now interesting to consider how the various criteria perform

Table 1: Test of the timestep criteria (69) to (71) for the integration of Kepler ellipses in the field of a point mass. The free parameters of the criteria are set such that they all integrate a circular orbit using the same number of timesteps. We then consider orbits of increasing eccentricity ϵ , keeping the total energy of the orbiting particle constant. Averaged over five orbits, the table lists the mean relative drift of the total energy, and the number in parenthesis gives the number of force computations per orbit. An ∞ -sign means that the integration catastrophically failed.

ϵ	A	B	C
0	$< 10^{-10}$ (50)	$< 10^{-10}$ (50)	$< 10^{-10}$ (50)
0.5	-3.0×10^{-3} (57)	-1.9×10^{-3} (50)	-5.5×10^{-3} (70)
0.8	-0.018 (82)	-0.038 (48)	-0.041 (158)
0.9	-0.034 (113)	∞	-0.076 (311)
0.99	-0.072 (352)	∞	∞

Table 2: Test of timestep criteria for the integration of orbits in the potential of a singular isothermal sphere. We set the free parameters of the criteria (69) to (71) such that they all need the same number of timesteps for a circular orbit. We then consider orbits with smaller velocity $v = \kappa V_c$ at apocenter. The table lists the mean relative drift of total energy over a time $2\pi V_c/a_0$. The number in parenthesis gives the number of force computations occurring over that time.

κ	A	B	C
0	$< 10^{-10}$ (50)	$< 10^{-10}$ (50)	$< 10^{-10}$ (50)
0.5	-8.3×10^{-4} (78)	2.3×10^{-4} (61)	-3.4×10^{-3} (85)
0.2	-7.7×10^{-3} (101)	0.035 (63)	-0.037 (132)
0.1	-0.021 (117)	-0.17 (99)	-0.13 (196)
0.05	-0.047 (135)	∞	-0.28 (341)

when the eccentricity ϵ of the orbit is increased. In Table 1, we show the drift in total energy per orbit (averaged over 5 orbits) and the number of force computations needed per orbit for the three timestep criteria. Interestingly, only criterion (A) is able to stably integrate orbits of very high eccentricity. Furthermore, it delivers higher accuracy than (C) at a smaller

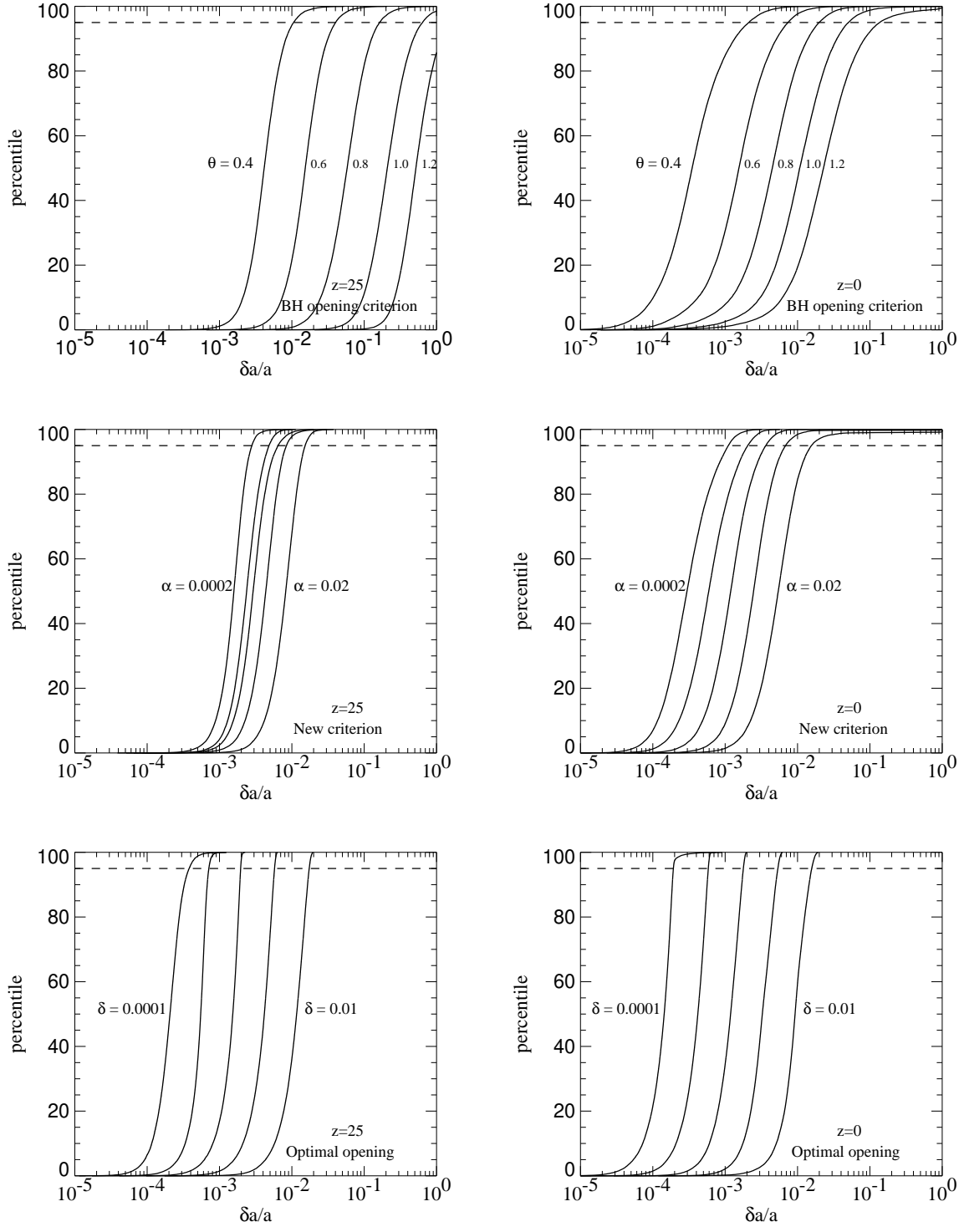


Figure 4: Cumulative distribution of the relative force error obtained as a function of the tolerance parameter for three opening criteria, and for two different particle distribution. The panels in the left column show results for the particle distribution in the initial conditions of a 32^3 simulation at $z = 25$, while the panels on the right give the force errors for the evolved and clustered distribution at $z = 0$.

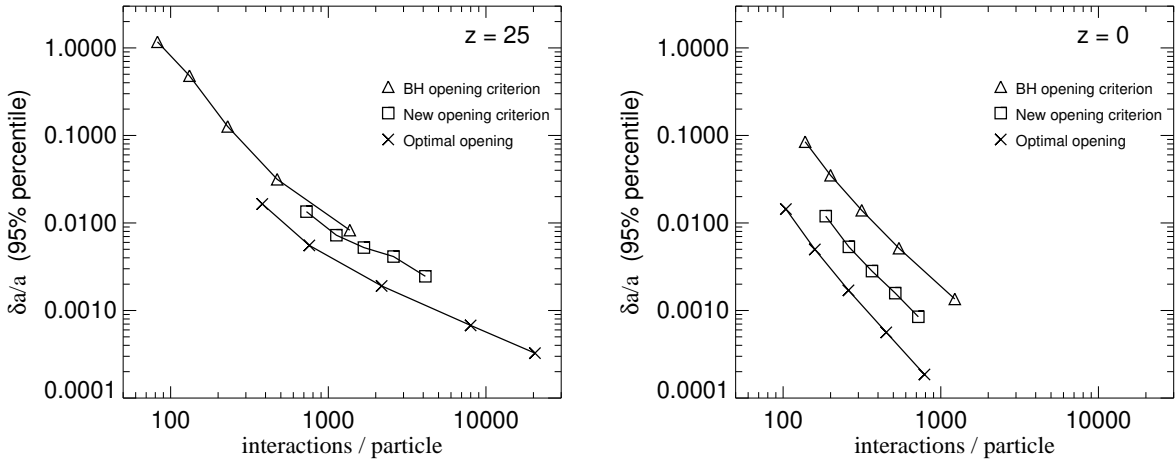


Figure 5: Computational efficiency of three different cell-opening criteria, parameterized by their tolerance parameters. The horizontal axes is proportional to the computational cost, and the vertical axes gives the 95% percentile of the cumulative distribution of relative force errors in a 32^3 cosmological simulation. The left panel shows results for the initial conditions at $z = 25$, the right panel for the clustered distribution at redshift $z = 0$.

computational cost. Similarly, (A) clearly outperforms (B), at least for $\epsilon \geq 0.5$.

Of larger relevance for cosmological N-body simulations is the potential of an isothermal sphere, which may serve as a simple approximation to a dark matter halo. Using the potential

$$\Phi(r) = -V_c^2 \left[\log \left(\frac{r}{a_0} \right) - 1 \right], \quad (72)$$

we perform a similar test as above. We set the free parameters of the timestep criteria such that they require 50 force computations for a circular orbit of radius a_0 . We now consider orbits with a velocity v at apocenter a_0 which is just a fraction $\kappa = v/V_c$ of the circular velocity. In Table 2, we list the mean relative drift of the total energy, given for a time interval $2\pi a_0/V_c$, and we list the number of force computations needed over that time. Again, the criterion (A) by far outperforms the other two criteria (B) and (C). For a relatively small number of force computations it provides both the best stability and the best accuracy for a given computational expense.

7.2. Force accuracy and opening criterion

In Section 3.3, we have pointed out that standard values of the BH-opening criterion can result in very high force errors for the initial conditions of cosmological N-body simulations. Here, the density field is very close to being homogeneous, so that small peculiar accelerations arise from a cancellation of relatively large partial forces. We now investigate this problem further using a cosmological simulation with 32^3 particles in a periodic box. We consider the particle distribution of

the initial conditions at redshift $z = 25$, and the clustered one of the evolved simulation at $z = 0$. Romeel Davé has kindly made these particle dumps available to us, together with exact forces he calculated for all particles with a direct summation technique, properly including the periodic images of the particles. In the following we will compare his forces (which we take to be the exact result) to the ones computed by the parallel version of GADGET using two processors on a Linux PC.

We first examine the distribution of the relative force error as a function of the tolerance parameter used in the two different cell-opening criterions (8) and (20). These results are shown in Figure 4, where we also contrast these distributions with the ones obtained with an *optimum* cell-opening strategy. The latter may be operationally defined as follows:

Any complete tree walk results in an interaction list that contains a number of internal tree nodes (whose multipole expansions are used) and a number of single particles (which give rise to exact partial forces). Obviously, the shortest possible interaction list is that of just one entry, the root node of the tree itself. Suppose we start with this interaction list, and then open always the one node of the *current* interaction list that gives rise to the largest absolute force error. This is the node with the largest difference between multipole expansion and exact force, as resulting from direct summation over all the particles represented by the node. With such an opening strategy, the shortest possible interaction list can be found for any desired level of accuracy. The latter may be set by requiring that the largest force error of any node in the interaction list has fallen below a fraction $\delta|\mathbf{a}|$ of the true force field.

Of course, this optimum strategy is not practical in a real simulation, after all it requires the knowledge of all the exact forces for all internal nodes of the tree. If these were known, we wouldn't have to bother with trees to begin with. However, it is extremely interesting to find out what such a fiducial optimum opening strategy would ultimately deliver. Any other analytic or heuristic cell-opening criterion is bound to be worse than it. It is then interesting to know how much worse such criteria are, because this will delineate the maximum performance improvement possible by adopting alternative cell-opening criteria. We therefore went through the exercise of computing exact direct summation forces for all internal nodes, for all particle positions, hence allowing us to perform an optimum tree walk in the above way. The resulting cumulative error distributions as a function of δ are shown in Figure 4.

Looking at this Figure, it is clear that the BH error distribution has a more pronounced tail of large force errors compared to our new opening criterion. What is most striking however is that at high redshift the BH force errors can become very large for values of the opening angle θ that tend to give perfectly acceptable accuracy for a clustered mass distribution. This is clearly caused by its purely geometrical nature, which does not 'know' about the smallness of the net forces, and thus not invest sufficient effort to evaluate partial forces to high enough accuracy.

The error distributions alone do not tell yet about the computational efficiency of the cell-opening strategies. To assess these, we define the error for a given cell-opening criterion as the 95% percentile of the error distribution, and we plot this versus the mean length of the interaction list per particle. This length is essentially linearly related to the computational cost of the force evaluation.

In Figure 5 we compare the performance of the cell-opening criteria in this way. At high redshift, we see that the large errors of the BH criterion are mainly caused because the mean length of the interaction list does not adapt properly to the more demanding requirements of the force computation in this regime. Our 'new' cell-opening criterion does much better in this respect; its errors remain well controlled without having to adjust the tolerance parameter.

Another advantage of the new criterion is that it is in fact more efficient than the BH criterion, i.e. it achieves higher force accuracy for a given computational expense. As Figure 5 shows, for a clustered particle distribution in a cosmological simulation, the implied saving can easily reach a factor 2-3, speeding up the simulation by the same factor. Similar performance improvements are obtained for isolated galaxies, as the example in Figure 6 demonstrates. This can be understood as follows: The geometrical BH criterion doesn't care about the dynamical significance of the mass distribution. For example, it will invest a large number of cell-particle interactions to compute the force exerted by a large void to a high relative accuracy, while actually this force is of small absolute size,

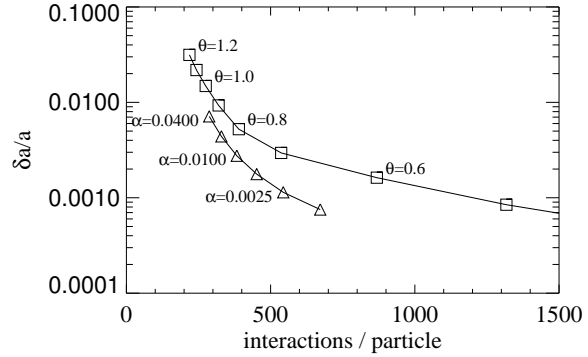


Figure 6: Force errors for an isolated halo/disk galaxy with the BH-criterion (boxes), and the new opening criterion (triangles). The plot shows the 90% percentile of the error distribution, i.e. 90% of the particles have force errors below the cited values. The horizontal axes measures the computational expense.

and it would be much better to concentrate on those regions that provide most of the force on the current particle. The new opening criterion follows this latter strategy, improving the force accuracy at a given number of particle-cell interactions.

We note that the improvement obtained by criterion (20) brings us about halfway to what might ultimately be possible with an optimum criterion. It appears that there is still room for further improvement of the cell-opening criterion, even if it is clear that the optimum can never quite be reached.

7.3. Colliding disk galaxies

As a test of the performance and accuracy of the integration of collisionless systems, we here consider a pair of merging disk galaxies. Each galaxy has a massive dark halo consisting of 30000 particles, and an embedded stellar disk, represented by 20000 particles. The dark halo is modeled according to the NFW-profile, adiabatically modified by the central exponential disk, which contributes 5% of the total mass. The halo has a circular velocity $v_{200} = 160 \text{ km s}^{-1}$, a concentration $c = 5$, and spin parameter $\lambda = 0.05$. The radial exponential scale length of the disk is $R_d = 4.5 \text{ h}^{-1} \text{kpc}$, while the vertical structure is that of an isothermal sheet with thickness $z_0 = 0.2R_d$. The gravitational softening of the halo particles is set to $0.4 \text{ h}^{-1} \text{kpc}$, and that of the disk to $0.1 \text{ h}^{-1} \text{kpc}$.

Initially, the two galaxies are set-up on a parabolic orbit, with separation such that their dark haloes just touch. Both of the galaxies have a prograde orientation, but are inclined with respect to the orbital plane. In fact, the test considered here corresponds exactly to the simulation 'C1' computed by Springel (2000), where more information about the construction of the initial conditions can be found (see also Springel

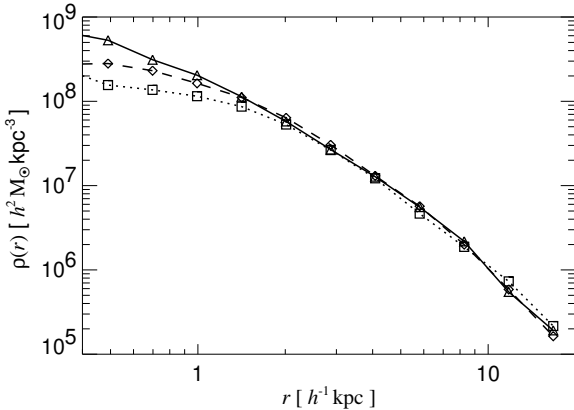


Figure 7: Spherically averaged density profile of the stellar component in the merger remnant of two colliding disk galaxies. Triangles show the results obtained using our variable timestep integration, while boxes and diamonds are for fixed timestep integrations with $\Delta t = 0.01$ and $\Delta t = 0.0025$, respectively. Note that the simulation using the adaptive timestep is about as expensive as the one with $\Delta t = 0.01$. In each case, the center of the remnant was defined as the position of the particle with the minimum gravitational potential.

& White, 1999).

We first consider a run of this model with a set of parameters equal to the coarsest values we would typically employ for a simulation of this kind. For the time integration, we used the parameter $\alpha_{\text{tol}}\sigma = 25 \text{ km s}^{-1}$, and for the force computation with the tree algorithm, the new opening criterion with $\alpha = 0.04$. The simulation was then run from $t = 0$ to $t = 2.8$ in internal units of time (corresponding to $2.85 h^{-1} \text{Gyr}$). During this time the galaxies have their first close encounter at around $t \simeq 1.0$, where tidal tails are ejected out of the stellar disks. Due to the braking by dynamical friction, the galaxies eventually fall together for a second time, after which they quickly merge and violently relax to form a single merger remnant. At $t = 2.8$, the inner parts of the merger remnant are well relaxed.

This simulation required a total number of 4684 steps and 27795733 force computations, i.e. a computationally equally expansive computation with fixed timesteps could just make 280 full timesteps. The relative error in the total energy was 3.0×10^{-3} , and a Sun Ultrasparc-II workstation did the simulation in 4 hours (using the serial code). Note that the raw force speed with ~ 2800 force computations per second was really very high – older workstations will achieve somewhat smaller values, of course.

We now consider a simulation of the same system using a fixed timestep. For $\Delta t = 0.01$, the run needs 280 full steps, i.e. it consumes the same amount of CPU time as above. However, in this simulation, the error in the total energy is

2.2%, substantially larger than before. There are also differences in the density profile of the merger remnants. In Figure 7, we compare the inner density profile of the simulation with adaptive timesteps (triangles) to the one with a fixed timestep of $\Delta t = 0.01$ (boxes). We here show the spherically averaged profile of the stellar component, with the center of the remnants defined as the position of the particle with the minimum gravitational potential. It can be seen that in the innermost $\sim 1 h^{-1} \text{kpc}$, the density obtained with the fixed timestep falls short of the adaptive timestep integration.

To get an idea how small the fixed timestep has to be to achieve similar accuracy as with the adaptive timestep, we have simulated this test a second time, with a fixed timesteps of $\Delta t = 0.0025$. We also show the corresponding profile (diamonds) in Figure 7. It can be seen that for smaller Δt , the agreement with the variable timestep result improves. At $\sim 2 \times 0.4 h^{-1} \text{kpc}$, the softening of the dark matter starts to become important. For agreement down to this scale, the fixed timestep needs to be slightly smaller than $\Delta t = 0.0025$, so the overall saving due to the use of individual particle timesteps is at least a factor of 4 – 5 in this example.

7.4. Collapse of a cold gas sphere

The self-gravitating collapse of an initially isothermal, cool gas sphere has been a common test problem of SPH codes (Evrard, 1988; Hernquist & Katz, 1989; Steinmetz & Müller, 1993; Thacker et al., 1998; Carraro et al., 1998, and others). Following these authors, we consider a spherically symmetric gas cloud of total mass M , radius R , and initial density profile

$$\rho(r) = \frac{M}{2\pi R^2} \frac{1}{r}. \quad (73)$$

We take the gas to be of constant temperature initially, with an internal energy per unit mass of

$$u = 0.05 \frac{GM}{R}. \quad (74)$$

At the start of the simulation, the gas particles are at rest. We obtain their initial coordinates from a distorted regular grid that reproduces the density profile (73), and we use a system of units with $G = M = R = 1$.

In Figure 8, we show the evolution of the potential, the thermal, and the kinetic energy of the system from the start of the simulation at $t = 0$ to $t = 3$. We plot results for two simulations, one with 30976 particles (solid), and one with 4224 particles (dashed). During the central bounce between $t \approx 0.8$ and $t \approx 1.2$ most of the kinetic energy is converted into heat, and a strong shock wave travels outward. Later, the system slowly settles to virial equilibrium.

For these runs N_s was set to 40, the gravitational softening to $\epsilon = 0.02$, and time integration was controlled by the

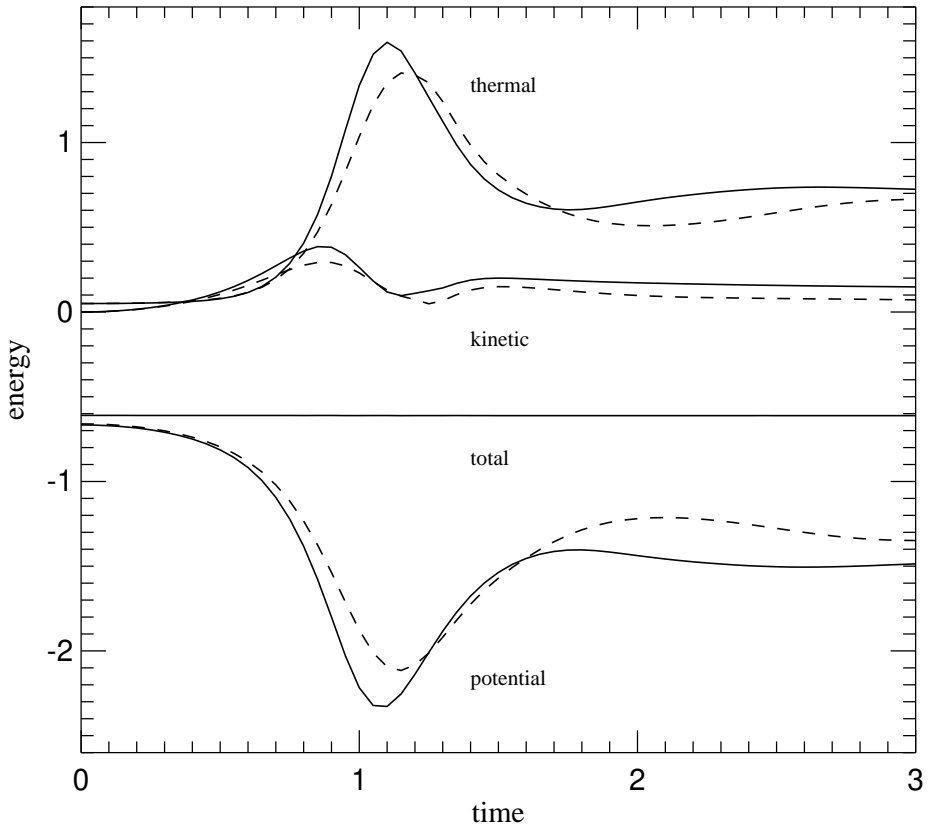


Figure 8: Time evolution of the thermal, kinetic, potential, and total energy for the collapse of an initially isothermal gas sphere. Solid lines show results for a simulations with 30976 particles, dashed lines are for a 4224 particle run.

parameters $\alpha_{\text{tol}}\sigma = 0.05$ and $\alpha_{\text{cour}} = 0.1^2$, resulting in very good energy conservation. The absolute error in the total energy is less than 1.1×10^{-3} at all times during the simulation, translating to a relative error of 0.23%. Since we use a time integration scheme with individual timesteps of arbitrary size, this small error is reassuring. The total number of small steps taken by the 4224 particle simulation was 3855, with a total of 2192421 force computations, i.e. the equivalent number of ‘full’ timesteps was 519. A Sun Ultrasparc-II workstation needed 2300 seconds for the simulation. The larger 30976 particle run took 10668 steps, with an equivalent of 1086 ‘full’ steps, and 12 hours of CPU time. Note that by reducing the time integration accuracy by a factor of 2, with a corresponding reduction of the CPU time consumption by the same factor, the results do practically not change, however, the maximum error in the energy goes up to 1.2% in this case.

²Note that our definition of the smoothing length h differs by a factor of 2 from most previous SPH implementations. As a consequence, corresponding values of α_{cour} are different by a factor of 2, too.

The results of Figure 8 agree very well with those of Steinmetz & Müller (1993), and with Thacker et al. (1998) if we compare to their ‘best’ implementation of artificial viscosity (their version 12). Steinmetz & Müller (1993) have also computed a solution of this problem with a very accurate, one-dimensional, spherically symmetric piecewise parabolic method (PPM). For particle numbers above 10000, our SPH results become very close to the finite difference result. However, even for very small particle numbers, SPH is capable of reproducing the general features of the solution very well. We also expect that a *three-dimensional* PPM calculation of the collapse would require substantially more CPU time than our SPH calculation.

7.5. Performance and scalability of the parallel gravity

We here show a simple test of the performance of the parallel version of the code under conditions relevant for real target applications. For this test, we have used a ‘stripped-down’

Table 3: Consumption of CPU-time in various parts of the code for a cosmological run from $z = 50$ to $z = 4.3$. The table gives timings for runs with 4, 8 and 16 processors on the Garching Cray T3E. The computation of the gravitational forces is by far the dominant computational task. We have further split up that time into the actual tree-walk time, the tree-construction time, the time for communication and summation of force contributions, and into the time lost by work-load imbalance. The potential computation is done only once in this test (it can optionally be done in regular intervals to check energy conservation of the code). ‘Miscellaneous’ refers to time spent in advancing and predicting particles, and in managing the binary tree for the timeline. I/O time for writing a snapshot file (groups of processors can write in parallel) is only 1-2 seconds, and therefore not listed here.

	4 processors	8 processors	16 processors			
	cumulative time [sec]	relative time	cumulative time [sec]	relative time	cumulative time [sec]	relative time
total	8269.0	100.0 %	4074.0	100.0 %	2887.5	100.0 %
gravity	7574.6	91.6 %	3643.0	89.4 %	2530.3	87.6 %
tree walks	5086.3	61.5 %	2258.4	55.4 %	1322.4	45.8 %
tree construction	1518.4	18.4 %	773.7	19.0 %	588.4	20.4 %
communication & summation	24.4	0.3 %	35.4	0.9 %	54.1	1.9 %
work-load imbalance	901.5	10.9 %	535.1	13.1 %	537.4	18.6 %
domain decomposition	209.9	2.5 %	158.1	3.9 %	172.2	6.0 %
potential computation (optional)	46.3	0.2 %	18.1	0.4 %	11.4	0.4 %
miscellaneous	438.3	5.3 %	254.8	6.3 %	173.6	6.0 %

version of the initial conditions originally constructed for a high-resolution simulation of a cluster of galaxies. The original set of initial conditions was set-up to follow the cosmological evolution of a large spherical region with comoving radius $70 h^{-1}\text{Mpc}$, within a ΛCDM cosmogeny corresponding to $\Omega_0 = 0.3$, $\Omega_\Lambda = 0.7$, $z_{\text{start}} = 50$, and $h = 0.7$. In the center of the simulation sphere, 2 million high-resolution particles were placed in the somewhat enlarged Lagrangian region of the cluster. The rest of the volume was filled with an extended shell of boundary particles of larger mass and larger softening; they are needed for a proper representation of the gravitational tidal field.

To keep our test simple, we have cut out a sphere of comoving radius $12.25 h^{-1}\text{Mpc}$ around the origin from these initial conditions, and we only simulated the 500000 high-resolution particles with mass $m_p = 1.36 \times 10^9 h^{-1}\text{M}_\odot$ found within this region. Such a simulation will not be useful for direct scientific analysis because it does not model the tidal field properly. However, this test will show realistic clustering and time-stepping behaviour, and thus allows a reasonable assessment of the expected computational cost and scaling of the full problem.

We have run the test problem with GADGET on the Garching T3E from redshift $z = 50$ to redshift $z = 4.3$. We repeated the identical run on partitions of size 4, 8, and 16 processors. In this test, we included quadrupole moments in the tree computation, we used a BH opening criterion with $\theta = 1.0$, and a gravitational softening length of $15 h^{-1}\text{kpc}$.

In Table 3 we list in detail the elapsed wall-clock time for various parts of the code for the three simulations. The dominant sink of CPU time is the computation of gravitational

forces for the particles. To advance the test simulation from $z = 50$ to $z = 4.3$, GADGET needed 30.0×10^6 force computations in a total of 3350 timesteps. Note that on average only 1.8% of the particles are advanced in a single timestep. Under these conditions it is challenging to eliminate sources of overhead incurred by the time-stepping and to maintain work-load balancing. GADGET solves this task satisfactorily. If we would use a fixed timestep, the work-load balancing would essentially be perfect. Note that the use of our adaptive timestep integrator results in a saving of about a factor of 3-5 compared to a fixed timestep scheme with the same accuracy.

We think that the overall performance of GADGET is quite good in this test. The raw gravitational speed is very high, and the algorithm used to parallelize the force computation scales well, as is seen in the upper left panel of Figure 9. Note that the force-speed of the $N_p = 8$ run is even higher than that of the $N_p = 4$ run. This is because the domain decomposition does exactly one split in the x -, y -, and z -directions in the $N_p = 8$ case. The domains are then close to cubes, which reduces the depth of the tree and speeds up the tree-walks.

Also, the force communication does not involve a significant communication overhead, and the time spent in miscellaneous tasks of the simulation code scales closely with processor number. Most losses of GADGET occur due to work-load imbalance in the force computation. While we think these losses are acceptable in the above test, one should keep in mind that we here kept the problem size *fixed*, and just increased the processor number. If we *also scale up the problem size*, work-load balancing will be significantly easier to achieve, and the efficiency of GADGET will be nearly as high

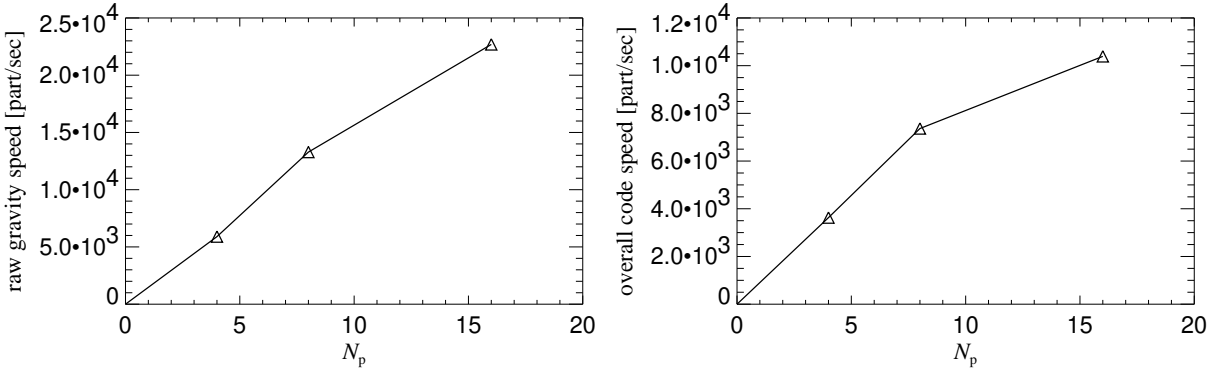


Figure 9: Code performance and scalability for a cosmological integration with vacuum boundaries. The left panel shows the speed of the gravitational force computation as a function of processor number (in particles per second). This is based on the tree walk time alone. In the simulation, additional time is needed for tree construction, work-load imbalance, communication, domain decomposition, prediction of particles, timeline, etc. This reduces the ‘effective’ speed of the code, as shown in the right panel. This effective speed gives the number of particles advanced by one timestep per second. Note that the only significant source of work-load imbalance in the code occurs in the gravity computation, where some small fraction of time is lost when processors idly wait for others to finish their tree-walks.

as for small processor number.

7.6. Parallel SPH in a periodic volume

As a further test of the scaling and performance of the parallel version of GADGET in typical cosmological applications we consider a simulation of structure formation in a periodic box of size $(50h^{-1}\text{Mpc})^3$, including adiabatic gas physics. We use 32^3 dark matter particles, and 32^3 SPH particles in a ΛCDM cosmology with $\Omega_0 = 0.3$, $\Omega_\Lambda = 0.7$ and $h = 0.7$, normalized to $\sigma_8 = 0.9$. For simplicity, initial conditions are constructed by displacing the particles from a grid, with the SPH particles placed on top of the dark matter particles.

We have evolved these initial conditions from $z = 10$ to $z = 1$, using 2, 4, 8, 16, and 32 processors on the Cray T3E in Garching. The final particle distributions of all these runs are in excellent agreement with each other.

In the bottom panel of Figure 10, we show the code speed as a function of the number of processors employed. We here define the speed as the total number of force computations divided by the total elapsed wall-clock time during this test. Note that the scaling of the code is almost perfectly linear in this example, even better than for the set-up used in the previous section. In fact, this is largely caused by the simpler geometry of the periodic box as compared to the spherical volume used earlier. The very absence of such boundary effects makes the periodic box easier to domain-decompose, and to work-balance.

The top and middle panels of Figure 10 show the speed of the gravitational force computation and that of the SPH part separately. What we find remarkable is that the SPH algorithm scales really very well, which is promising for future

large-scale applications.

It is interesting that in this test (where $N_s = 40$ SPH neighbours have been used) the hydrodynamical part actually consumes only $\sim 25\%$ of the overall CPU time. Partly this is due to the slower gravitational speed in this test compared to the results shown in Figure 9, which in turn is caused by the Ewald summation needed to treat the periodic boundary conditions, and by longer interaction lists in the present test (we here used our new opening criterion). Also note that only half the particles in this simulation are SPH particles.

We remark that the gravitational force computation will usually be more expensive at higher redshift than at lower redshift, while the SPH part does not have such a dependence. When the material becomes more clustered, the fraction of time consumed by the SPH part tends to increase somewhat. However, this is then not because the SPH becomes slower, but because gravity becomes faster. On the other hand, in dissipative simulations one will typically form clumps of cold gas with very high density - objects that we think will form stars and turn into galaxies. Such cold knots of gas can slow down the computation substantially, because they require small hydrodynamical timesteps, and if a lower spatial resolution cut-off for SPH is imposed, the hydrodynamical smoothing may start to involve more neighbours than N_s .

8. Discussion

We have presented the numerical algorithms of our new code GADGET, designed as a flexible tool to study a wide range of problems in cosmology. Typical applications of GADGET can include interacting and colliding galaxies, star formation

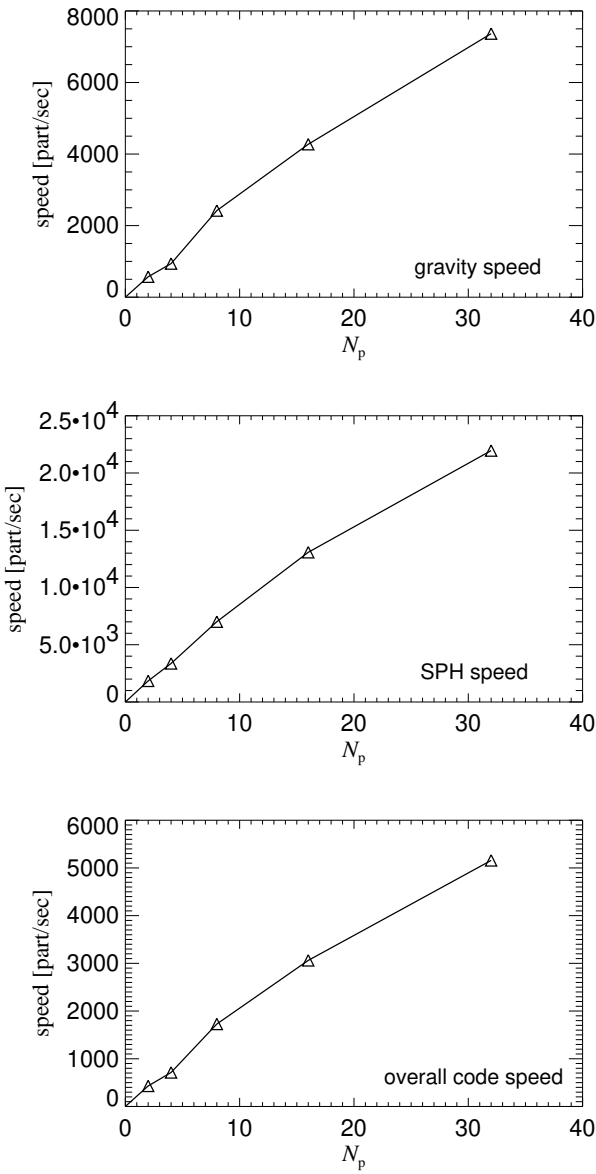


Figure 10: Speed of the code in a gasdynamical simulation of a periodic Λ CDM universe, run from $z = 10$ to $z = 1$, as a function of the number of T3E processors employed. The top panel shows the speed of the gravitational force computation (including tree construction times). We define the speed here as the number of force computations per elapsed wall-clock time. The middle panel gives the speed in the computation of hydrodynamical forces, while the bottom panel shows the resulting overall code speed in terms of particles advanced by one timestep per second. This effective code speed includes all other code overhead, which is less than 5% of the total cpu time in all runs.

and feedback in the interstellar medium, formation of clusters of galaxies, or the formation of large-scale structure in the

universe.

In fact, GADGET has already been used successfully in all of these areas. Using our code, Springel & White (1999) have studied the formation of tidal tails in colliding galaxies, and Springel (2000) has modeled star formation and feedback in isolated and colliding gas-rich spirals. For these simulations, the serial version of the code was employed, both with and without support by the GRAPE special-purpose hardware.

The parallel version of GADGET has been used to compute high-resolution N-body simulations of clusters of galaxies (Springel et al., 1999; Yoshida et al., 2000). In the largest simulation of this kind, 69 million particles have been employed, with 20 million of them ending up in the virialized region of a single object. The particle mass in the high-resolution zone was just 10^{-10} of the total simulated mass, and the gravitational softening length was $0.7 h^{-1}$ kpc in a simulation volume of diameter $140 h^{-1}$ Mpc, translating to an impressive spatial dynamic range of 2×10^5 in three dimensions.

We have also successfully employed GADGET for two ‘constrained-realization’ (CR) simulations of the Local Universe. In these simulations, the observed density field as seen by IRAS galaxies has been used to constrain the phases of the waves of the initial fluctuation spectrum. For each of the two CR simulations, we employed ~ 75 million particles in total, with 53 million high-resolution particles of mass $3.6 \times 10^9 h^{-1} M_\odot$ (Λ CDM) or $1.2 \times 10^{10} h^{-1} M_\odot$ (τ CDM) in the low-density and critical-density models, respectively.

The main technical features of GADGET are as follows. Gravitational forces are computed with a Barnes & Hut octree, using multipole expansions up to quadrupole order. Periodic boundary conditions can optionally be used and are implemented by means of Ewald summation. The cell-opening criterion may be chosen either as the standard BH-criterion, or a new criterion which we have shown to be computationally more efficient and better suited to cosmological simulations starting at high redshift. As an alternative to the tree-algorithm, the serial code can use the special-purpose hardware GRAPE both to compute gravitational forces and for the search of SPH neighbours.

In our SPH implementation, the number of smoothing neighbors is either kept exactly constant (only in the serial code), or is allowed to fluctuate in a small band. Using a suitable neighbour searching algorithm, we can guarantee that always all interacting pairs of SPH particles are found, thereby ensuring force antisymmetry and momentum conservation. We use a shear-reduced artificial viscosity that has emerged as a very good parameterization in recent systematic studies that compared several alternative formulations (Thacker et al., 1998; Lombardi et al., 1999).

Parallelization of the code for massively parallel supercomputers is achieved in an explicit message passing approach, using the MPI standard communication library. The simulation volume is spatially split in a recursive orthogonal

bisection, and each of the resulting domains is mapped onto one processor. Dynamic work-load balancing is achieved by measuring the computational expense incurred by each particle, and balancing the sum of these weights in the domain decomposition.

The code allows fully adaptive, individual particle timesteps, both for collisionless particles and for SPH particles. The speed-up obtained by the use of individual timesteps depends on the dynamic range of the time scales present in the problem, and on the relative population of these time scales with particles. For a collisionless cosmological simulation with a gravitational softening length larger than $\sim 30 h^{-1}\text{kpc}$ the overall saving is typically a factor of 3 – 5. However, if smaller softening lengths are desired, the use of individual particle timesteps results in larger savings. In the hydrodynamical part, the savings can be still larger, especially if dissipative physics is included. In this case, adaptive timesteps may be required to make a simulation feasible to begin with. For collisionless particles, we use a timestep criterion based on the inverse of the particle acceleration. We have shown that this criterion outperforms simple alternative criteria that are currently in use. GADGET can be used to run simulations both in physical and in comoving coordinates. The latter is used for cosmological simulations only. Here, the code employs an integration scheme that can deal with arbitrary cosmological background models, and which is exact in linear theory, i.e. the linear regime can be traversed with maximum efficiency.

GADGET is an intrinsically Lagrangian code. Both the gravity and the hydrodynamical parts impose no restriction on the geometry of the problem, nor any hard limit on the allowable dynamic range. Current and future simulations of structure formation that aim to resolve galaxies in their correct cosmological setting will have to resolve length scales of size $0.1 - 1 h^{-1}\text{kpc}$ in volumes of size $\sim 100 h^{-1}\text{Mpc}$. This range of scales is accompanied by a similarly large dynamic range in mass and time scales. Our new code is essentially free to adapt to these scales naturally, and it invests computational work only where it is needed. It is therefore a tool that should be well suited to work on these problems.

Since GADGET is written in standard ANSI-C, and the parallelization for massively parallel supercomputers is achieved with the standard MPI library, the code runs on a large variety of platforms, without requiring any change. Having eliminated the dependence on proprietary compiler software and operating systems we hope that the code will remain usable for the foreseeable future. We release the parallel and the serial version of GADGET publically in the hope that they will be useful for others as a scientific tool, and that broader use will provide a basis for further numerical improvements.

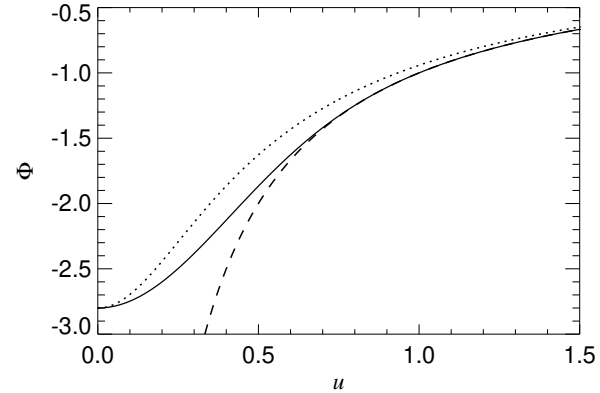


Figure 11: Comparison of spline-softened (solid) and Plummer-softened (dotted) potential of a point mass with the Newtonian potential (dashed). Here $h = 1.0$, and $\epsilon = h/2.8$.

Acknowledgements

We are grateful to Barbara Lanzoni, Bepi Tormen, and Simone Marri for their patience in working with earlier versions of GADGET. We thank Lars Hernquist, Martin White, Charles Coldwell, Jasjeet Bagla and Matthias Steinmetz for many helpful discussions on various algorithmic and numerical issues. We also thank Romeel Davé for making some of his test particle configurations available to us. We are indebted to the Rechenzentrum of the Max-Planck-Society in Garching for providing excellent support for their T3E, on which a large part of the computations of this work have been carried out.

Appendix: Softened tree nodes

The smoothing kernel we use for SPH calculations is a spline of the form (Monaghan & Lattanzio, 1985)

$$W(r; h) = \frac{8}{\pi h^3} \begin{cases} 1 - 6\left(\frac{r}{h}\right)^2 + 6\left(\frac{r}{h}\right)^3, & 0 \leq \frac{r}{h} \leq \frac{1}{2}, \\ 2\left(1 - \frac{r}{h}\right)^3, & \frac{1}{2} < \frac{r}{h} \leq 1, \\ 0, & \frac{r}{h} > 1. \end{cases} \quad (75)$$

Note that we define the smoothing kernel on the interval $[0, h]$ and not on $[0, 2h]$ as it is frequently done in other SPH calculations.

We derive the spline-softened gravitational force from this kernel by taking the force from a point mass m to be the one resulting from a density distribution $\rho(\mathbf{r}) = mW(\mathbf{r}; h)$. This leads to a potential

$$\Phi(\mathbf{r}) = G \frac{m}{h} W_2\left(\frac{r}{h}\right) \quad (76)$$

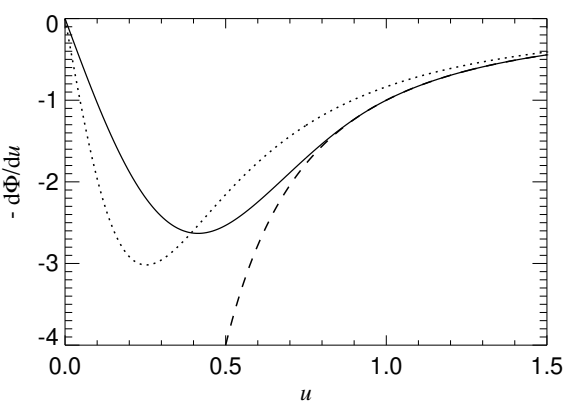


Figure 12: Comparison of spline-softened (solid) and Plummer-softened (dotted) force law with Newton’s law (dashed). Here $h = 1.0$, and $\epsilon = h/2.8$.

with a kernel

$$W_2(u) = \begin{cases} \frac{16}{3}u^2 - \frac{48}{5}u^4 + \frac{32}{5}u^5 - \frac{14}{5}, & 0 \leq u < \frac{1}{2}, \\ \frac{1}{15u} + \frac{32}{3}u^2 - 16u^3 + \frac{48}{5}u^4 - \frac{32}{15}u^5 - \frac{16}{5}, & \frac{1}{2} \leq u < 1, \\ -\frac{1}{u}, & u \geq 1. \end{cases} \quad (77)$$

The multipole expansion of a group of particles is discussed in Section 3.1. It results in a potential and force given by equations (13) and (17), respectively. The functions appearing in equation (17) are defined as

$$g_1(y) = \frac{g'(y)}{y}, \quad (78)$$

$$g_2(y) = \frac{g''(y)}{y^2} - \frac{g'(y)}{y^3}, \quad (79)$$

$$g_3(y) = \frac{g'_2(y)}{y}, \quad (80)$$

$$g_4(y) = \frac{g'_1(y)}{y}. \quad (81)$$

Writing $u = y/h$, the explicit forms of these functions are

$$g_1(y) = \frac{1}{h^3} \begin{cases} -\frac{32}{3} + \frac{192}{5}u^2 - 32u^3, & u \leq \frac{1}{2}, \\ \frac{1}{15u^3} - \frac{64}{3} + 48u - \frac{192}{5}u^2 + \frac{32}{3}u^3, & \frac{1}{2} < u < 1, \\ -\frac{1}{u^3}, & u > 1, \end{cases} \quad (82)$$

$$g_2(y) = \frac{1}{h^5} \begin{cases} \frac{384}{5} - 96u, & u \leq \frac{1}{2}, \\ -\frac{384}{5} - \frac{1}{5u^5} + \frac{48}{u} + 32u, & \frac{1}{2} < u < 1, \\ \frac{3}{u^5}, & u > 1, \end{cases} \quad (83)$$

$$g_3(y) = \frac{1}{h^7} \begin{cases} -\frac{96}{u}, & u \leq \frac{1}{2}, \\ \frac{32}{u} + \frac{1}{u^7} - \frac{48}{u^3}, & \frac{1}{2} < u < 1, \\ -\frac{15}{u^7}, & u > 1, \end{cases} \quad (84)$$

$$g_4(y) = \frac{1}{h^5} \begin{cases} -\frac{96}{5}(5u - 4), & u \leq \frac{1}{2}, \\ \frac{48}{u} - \frac{1}{5u^5} - \frac{384}{5} + 32u, & \frac{1}{2} < u < 1, \\ \frac{3}{u^5}, & u > 1. \end{cases} \quad (85)$$

In Figures 11 and 12, we show the spline-softened and Plummer-softened force and potential of a point mass. For a given spline softening length h , we define the ‘equivalent’ Plummer softening length as $\epsilon = h/2.8$. For this choice, the minimum of the potential at $u = 0$ has the same depth.

References

Athanassoula E., Bosma A., Lambert J. C., Makino J., 1998, MNRAS, 293, 369
 Bagla J. S., 1999, preprint, astro-ph/9911025
 Balsara D. W., 1995, J. Comp. Phys., 121, 357
 Barnes J., Hut P., 1986, Nature, 324, 446
 Bode P., Ostriker J. P., Xu G., 1999, preprint, astro-ph/9912541
 Carraro G., Lia C., Chiosi C., 1998, MNRAS, 297, 1021
 Couchman H. M. P., 1991, ApJ, 368, 23
 Couchman H. M. P., Thomas P., Pearce F., 1995, ApJ, 452, 797
 Davé R., Dubinski J., Hernquist L., 1997, New Astronomy, 2, 277
 Dikaiakos M. D., Stadel J., 1995, in preparation
 Dubinski J., 1996, New Astronomy, 1, 133
 Dubinski J., Mihos J. C., Hernquist L., 1996, ApJ, 462, 576
 Ebisuzaki T., Makino J., Fukushige T., et al., 1993, PASJ, 45, 269
 Efstathiou G., Davis M., Frenk C. S., White S. D. M., 1985, ApJS, 57, 241
 Evrard A. E., 1988, MNRAS, 235, 911
 Frenk C. S., White S. D. M., Bode P., et al., 1999, ApJ, 525, 554
 Fukushige T., Ito T., Makino J., Ebisuzaki T., Sugimoto D., Umemura M., 1991, PASJ, 43, 841
 Gingold R. A., Monaghan J. J., 1977, MNRAS, 181, 375
 Groom W., 1997, The formation and evolution of galaxies in a cold dark matter universe, Ph.D. thesis, University of Cambridge
 Heller C. H., Shlosman I., 1994, ApJ, 424, 84
 Hernquist L., Bouchet F. R., Suto Y., 1991, ApJS, 75, 231
 Hernquist L., Katz N., 1989, ApJ, 70, 419
 Hiotelis N., Voglis N., 1991, A&A, 243, 333
 Hultman J., Källander D., 1997, A&A, 324, 534
 Jernigan J. G., Porter D. H., 1989, ApJS, 71, 871

Kang H., Ostriker J. P., Cen R., et al., 1994, *ApJ*, 430, 83

Katz N., Weinberg D. H., Hernquist L., 1996, *ApJS*, 105, 19

Klein R. I., Fisher R. T., McKee C. F., Truelove J. K., 1998, in *Proceedings of the International Conference on Numerical Astrophysics 1998 (NAP98)*, edited by S. M. Miyama, K. Tomisaka, T. Hanawa, p. 131, Kluwer Academic, Boston, Mass.

Kravtsov A. V., Klypin A. A., Khokhlov A. M. J., 1997, *ApJS*, 111, 73

Lia C., Carraro G., 1999, preprint, astro-ph/9912098

Lombardi J. C., Sills A., Rasio F. A., Shapiro S. L., 1999, *J. of Comp. Phys.*, 152, 687

Lucy L. B., 1977, *AJ*, 82, 1013

MacFarland T., Couchman H. M. P., Pearce F. R., Pichlmeier J., 1998, *New Astronomy*, 3, 687

Makino J., Funato Y., 1993, *PASJ*, 45, 279

Makino J., Taiji M., Ebisuzaki T., Sugimoto D., 1997, *ApJ*, 480, 432

Monaghan J. J., 1992, *Ann. Rev. Astron. Astrophys.*, 30, 543

Monaghan J. J., Gingold R. A., 1983, *J. Comp. Phys.*, 52, 374

Monaghan J. J., Lattanzio J. C., 1985, *A&A*, 149, 135

Navarro J. F., White S. D. M., 1993, *MNRAS*, 265, 271

Nelson R. P., Papaloizou J. C. B., 1994, *MNRAS*, 270, 1

Norman M. L., Bryan G. L., 1998, in *Proceedings of the International Conference on Numerical Astrophysics 1998 (NAP98)*, edited by S. M. Miyama, K. Tomisaka, T. Hanawa, p. 19, Kluwer Academic, Boston, Mass.

Pacheco P. S., 1997, *Parallel Programming with MPI*, Morgan Kaufmann Publishers, San Francisco

Pearce F. R., Couchman H. M. P., 1997, *New Astronomy*, 2, 411

Press W. H., Teukolsky S. A., Vetterling W. T., Flannery B. P., 1995, *Numerical recipies in C*, Cambridge University Press, Cambridge

Quinn T., Katz N., Stadel J., Lake G., 1997, preprint, astro-ph/9710043

Salmon J. K., Warren M. S., 1994, *J. Comp. Phys.*, 111, 136

Snir M., Otto S. W., Huss-Lederman S., Walker D. W., Dongarra J., 1995, *MPI: The complete reference*, MIT Press, Cambridge

Springel V., 2000, *MNRAS*, in press

Springel V., White S. D. M., 1999, *MNRAS*, 307, 162

Springel V., White S. D. M., Tormen G., Kauffmann G., 1999, *MNRAS*, in preparation

Spurzem R., 1997, in *Proc. Int. Symp. on Supercomputing - New Horizon of Computational Science*, edited by T. Ebisuzaki, Kluwer, Dordrecht

Steinmetz M., 1996, *MNRAS*, 278, 1005

Steinmetz M., Müller E., 1993, *A&A*, 268, 391

Thacker R. J., Tittley E. R., Pearce F. R., Couchman H. M. P., Thomas P. A., 1998, preprint, astro-ph/9809221

Theuns T., Rathsack M. E., 1993, *Comp. Phys. Comm.*, 76, 141

Viturro H. R., Carpintero D. D., 2000, *A& AS*, 142, 157

Warren M. S., Quinn P. J., Salmon J. K., Zurek W. H., 1992, *ApJ*, 399, 405

Wirth N., 1986, *Algorithms and data structures*, Prentice-Hall, London

Yoshida N., Springel V., White S. D. M., Tormen G., 2000, preprint, astro-ph/0002362